MODELING OF THE CRYOGENIC LIQUID POOL EVAPORATION AND THE EFFECT OF THE CONVECTIVE HEAT TRANSFER FROM ATMOSPHERE

A Thesis

by

WAQAS NAWAZ

Submitted to the Office of Graduate and Professional Studies of
Texas A&M University
in partial fulfillment of the requirements for the degree of

MASTER OF SCIENCE

Chair of Committee,	Luc Véchot
Co-Chair of Committee,	Marcelo Castier
Committee Member,	Hazem Nounou
Head of Department,	M. Nazmul Karim

May 2014

Major Subject: Chemical Engineering

ABSTRACT

Liquefied Natural Gas (LNG) has recently known significant development worldwide. The assessment and the control of the risks associated to the production, storage and transportation of LNG is of paramount importance to ensure the sustainability of this activity. This includes the prediction of the consequences of potential loss of containment of LNG, which requires the modelling of the vaporization rate of LNG resulting from the heat transfer between the pool and surroundings. The present work focuses on the role of evaporation and convection phenomena on the cryogenic pool temperature and its vaporization rate. Various models describing heat transfer by evaporation were compared. The models differ from each other in terms of mass transfer coefficient and saturation vapor pressure (i.e. linear versus logarithmic expression). Simulations were performed to observe the temperature and vaporization rate of cryogenic liquid pool (methane/nitrogen) under known atmospheric conditions. The results show that the pool initially stays at its boiling temperature, for models using linear driving force, such indicating the prevalence of boiling on the overall vaporization rate. Subsequently, the temperature of the cryogenic pool drops down, as the heat taken by evaporation exceeds the heat transfer by convection or conduction whereas, models adopting logarithmic driving force show drop in temperature from the beginning of simulation. The results of these models were compared to existing experimental data for cryogenic liquid vaporization rate to assess their accuracy and clarify the role of evaporation in the vaporization of a cryogenic liquid pool.

DEDICATION

I dedicate this thesis to my parents. I hope my achievements will bring joy on your faces and a sense of accomplishment of the dream you had for me.

ACKNOWLEDGEMENTS

I sincerely feel obliged to recognize the efforts of my advisor Dr. Luc Véchot, who has not only provided guidance in my research work but has helped me through.my tough times in life. I would like to acknowledge my committee members: Dr. Marcelo Castier and Dr. Hazem Nounou. I want to thank Dr. Tomasz Olewski without whom it would have never been possible.

I would also like to appreciate the support of all members of Mary Kay O'Connor Process Safety Center extension in Qatar. I want to acknowledge the long term, not only financial, support provided by BP Global Gas SPU for the LNG safety research, and the support of Qatar Petroleum in the form of the utilization of facilities and staff.

Finally, I would like to thank Ms. Alisha Basha and Dr. Valeria Casson Moreno for being moral support throughout.

NOMENCLATURE

DNV	Det Norske Veritas, (Norwegian Classification Society)
LNG	Liquefied natural gas
LN_2	Liquefied nitrogen
ODE	Ordinary differential equation
RLIC	Ras Laffan Industrial City
TAMUQ	Texas A&M University at Qatar
TNO	Toegepast Natuurwetenscheppelijk Onderzoek, (Netherlands Organization for Applied Scientific Research)
A	Area of pool, m^2
C	Constant for mass transfer coefficient obtained from experiment, -
C_P	Heat capacity of the substance, J kg^{-1} K^{-1}
C_{Pa}	Atmospheric specific heat capacity, J kg^{-1} K^{-1}
d	Power of velocity of air, -
D_{ac}	Diffusion coefficient of air and vapor, m^2 s^{-1}
e	Power of diameter of the pool, -
E_{vap}	Vaporization rate due to evaporation, kg s^{-1}
$f(x)$	Function of the mole fraction of vapor at pool surface, -
H_V	Heat of vaporization of the substance, J kg^{-1}
K'	Corrected mass transfer coefficient, m s^{-1}
K_m	Mass transfer coefficient, m s^{-1}

K_s	Thermal conductivity of the surface, W m^{-1} K^{-1}
L	Diameter of the pool, m
M	Mass of the pool at that time, kg
M_A	Molecular weight of species 1, kg $kmol^{-1}$
M_B	Molecular weight of species 2, kg $kmol^{-1}$
M_w	Molecular weight of vapor, kg $kmol^{-1}$
n	Function of ground roughness and temperature profile, -
N_u	Nusselt Number, -
P	Atmospheric pressure, atm
P_a	Atmospheric pressure, Pa
P_p	Partial pressure of the liquid in air, Pa
P_r	Prandtl number, -
P_v	Vapor pressure of the liquid, Pa
Q_{cond}	Heat flow rate from conduction, kW
Q_{conv}	Heat flow rate from conduction, kW
Q_{evap}	Heat flow rate from evaporation, kW
r	Radius of the pool, m
R	Universal gas constant, J $kmol^{-1}$ K^{-1}
R_e	Reynold number, -
S_c	Schmidt number, -
t	Time, s
T	Temperature of the Pool, K

T_a	Atmospheric temperature, K
T_m	Mean temperature of pool and air, K
T_s	Surface temperature, K
$\check{U}$	Velocity at the required height, m^{-1}
U_*	Atmospheric friction velocity, m s^{-1}
$\check{U}_1$	Known velocity at height z_1, m s^{-1}
$\check{U}_m$	Mean velocity of air, m s^{-1}
V_c	Vapor Concentration, kg m^{-3}
X	Mole fraction of specific component in pool, -
X_s	Surface roughness factor, -
z	Height at which $\check{U}$ is required, m
z_0	Surface roughness length, m
z_1	Height at which $\check{U}_1$ is calculated, m

Other Symbols

α_s	Thermal diffusivity of the surface, m^2 s^{-1}
λ_a	Thermal conductivity of air, W m^{-1} K^{-1}
μ_a	Atmospheric dynamic viscosity, kg m^{-1} s^{-1}
ρ_a	Density of air, kg m^{-3}
σ_{AB}	Collision diameter, Å
$\Omega_{D_{ac}}$	Collision Integral of Diffusion, -

TABLE OF CONTENTS

Page

LIST OF FIGURES

Page

LIST OF TABLES

Page

1. INTRODUCTION

In the process industry, many light chemical substances (normally in a gaseous state at ambient temperature and ambient pressure) are stored as liquids. Gases are liquefied either under high pressure or a very low temperature. The liquefaction drastically reduces the volume of the material, making it easier to store and transport. Natural gas is one of the best examples to be given in this context. LNG is the preferred solution for the storage and transportation of natural gas. This is particularly true in cases involving long distance transportation of the gas which makes pipeline transportation uneconomical or even impossible.

In 2012, the world's natural gas production and consumption grew by 1.9 % and 2.2 %, respectively. Qatar recorded a significant increase of 7.8 % in the production rate of natural gas. On the other hand, the growth rate of natural gas trade across the globe was extremely low, 0.1 %, whereas the global trade of LNG fell for the first time by -0.9 %. Even though there was a decline in the trade of LNG across the world, the export rate of LNG in Qatar grew by 4.7 % [1].

In 2010, Qatar became the largest producer and exporter of LNG in the world. Although the LNG industry across the world has a comparatively good safety record, the size and extent of LNG production in Qatar brings new challenges and requires special attention. Therefore, it is crucial to conduct fundamental and applied research in areas related to safe LNG production, handling and transportation in order to assure the sustainability of LNG industry in the State of Qatar as well as around the world.

The liquefaction of natural gas is done by cooling the gas below its boiling point (about -162°C), which reduces its volume by a factor of 650. LNG, being a cryogen, vaporizes rapidly upon contact with land or water in the case of accidental release. This may lead to fires or explosions as LNG is highly flammable. The prediction of the consequences of LNG loss of containment is critical to the assessment of the risks associated to LNG facilities. LNG spill consequence modelling involves the determination of the LNG vapor production rate (*source term modelling*) and its atmospheric dispersion downwind (*dispersion modelling*). The results of the dispersion modelling provide key information on the impact of accidental LNG release on given sensitive areas (e.g. surrounding population and facilities). Since the source term modelling defines the state of discharge, the discharge quantity and the discharge rate, its outcomes work as input parameters to the dispersion models which calculates the maximum distance vapors travel, the concentration zones as function of time and position. Hence an incorrect estimate of the source term will result in wrong approximations of the dispersion term.

The source term modelling in the case of LNG spills is directly related to the heat transfer between the cryogenic pool and the surroundings. Several heat transfer mechanisms are to be considered namely: radiation, conduction, convection and evaporative cooling. This research aims to improve source term modeling by specifically looking at the prediction of the effect of convection and evaporative cooling on LNG source term. The successful prediction of the source term will ultimately contribute to ensure the safety of LNG facilities through high quality risk assessments.

2. SCOPE OF WORK

The objective of this work is to perform the verification of existing evaporation models used for the prediction of the vaporization of cryogenic pool following an accidental spill on land. The challenge lies in the fact that the existing models have been developed essentially for non-boiling liquids.

The verification work starts with the building of a modelling tool using MATLAB software to simulate a cryogenic liquid spills over a solid uniform substrate under given atmospheric conditions (wind speed and ambient temperature). The simulation tool needs to be verified (comparison against existing software package) prior its use. The computational effectiveness and accuracy of the models are then identified using the tool.

A comprehensive set of simulation were performed for liquid methane spills over a solid substrate. The sensitivity of the results to the following model parameters is performed: type of substrate, wind speed, ambient temperature and liquid pool radius. The pool radius is assumed time-independent in order to simplify calculations and reduce computational time.

The evaporation models are subsequently validated again experimental data performed with liquid nitrogen under controlled conditions. They are however unfortunately very limited and performed at rather small scale. The understanding of the scaling properties is important in that context and thus is discussed.

This research should address the following questions in order to achieve its objectives:

- Is evaporation possible during accidents involving the loss of containment of cryogenic liquid?
- What is the minimum period of the spill duration that will lead to LNG pool vaporization transition from boiling to evaporation regime?
- Which model of evaporation can be considered computationally effective?
- Can we use models developed for non-cryogenic pools for cryogenic pools?
- What is the effect of wind speed on the heat flux provided and taken due to convection and evaporation respectively knowing that both are the function of wind speed?
- What is the effect of pool size on the vaporization of the cryogenic pool?
- What is the effect of ambient temperature on the vaporization of the cryogenic pool?
- What will be the effect of varying the type of substrate below the pool?

If the answers to these questions are established, the research can be taken to the next level where large scale experiment can be designed in order to provide data for the validation of models.

3. LITERATURE REVIEW

When a cryogen is spilled on the solid surface, the pool heat sources are the radiation from the sun, conduction from the ground, convection and evaporation from the air as shown in Figure 1. Radiation has been proved to be a small contributor to the cryogenic liquid vaporization rate and may be even additionally limited by the layers of the vapors formed above the surface of the liquid pool [2].

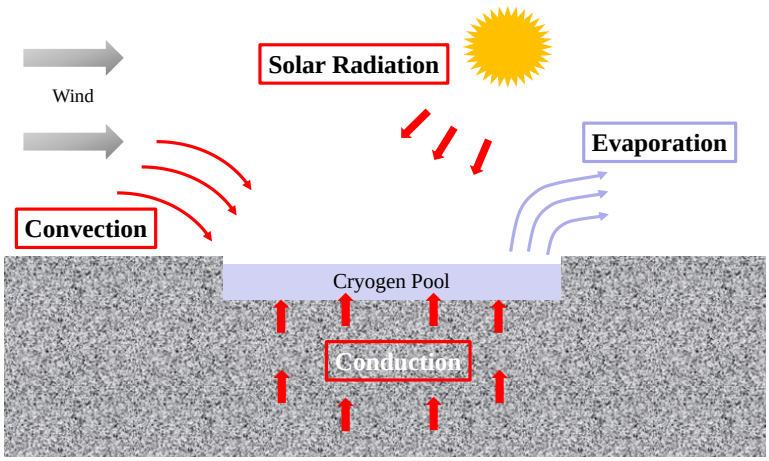

Figure 1: Heat transfer mechanisms involved in vaporization of a cryogenic liquid

3.1 Heat Flow Rate to the Liquid Pool by Conduction

At the initial stage of the spill, the conduction mode of heat transfer dominates other mechanisms due to a very high temperature gradient between the cryogenic pool and the substrate (i.e. concrete, soil). The model to describe the heat flow rate due to conduction from the ground to the cryogenic pool was adopted from Carslaw and Jaeger [3]. This model assumes a uniform semi-infinite solid medium with temperature

independent thermal properties and ideal contact of liquid with the ground, the later lead to a constant temperature of the ground's surface immediately after the spill. **The liquid pool temperature is assumed independent of time and is equal to a boiling point of the liquid**. This model leads to following conductive heat transfers to the pool

$$Q_{cond} = \frac{\pi\, r^2\, \chi_s\, k_s\, (T_s - T)}{1000\, t^{0.5} (\pi\, \alpha_s)^{0.5}} \qquad 1$$

where,

χ_s Surface roughness factor, dimensionless

k_s Thermal conductivity of the surface, W m^{-1} K^{-1}

T_s Temperature of the substrate at infinite depth, K

t Time, s

α_s Thermal diffusivity of the surface, m^2 s^{-1}

Q_{cond} Heat flow rate from conduction, kW

Thermal conductivity and thermal diffusivity are considered constant, independent of temperature, and are shown in Table 1 for different type of surfaces. In reality, the temperature of the surface of substrate cools down with time and the contribution of conduction decreases. With that decrease in conduction heat flux, the convection heat transfer mode starts to provide sufficient amount of heat to the pool that cannot be neglected [4].

Table 1: Surface data for different surface types [5]

Surface	Roughness Factor X_s	Thermal Conductivity K_s, W m^{-1} K^{-1}	Thermal Diffusivity α_s, m^2 s^{-1}
Concrete	1.00	1.21	5.72×10^{-7}
Insulating Concrete	1.00	0.22	8.27×10^{-7}
Wet Soil	2.63	2.21	9.48×10^{-7}
Dry Soil	2.63	0.32	8.27×10^{-7}

3.2 Heat Flow Rate to the Liquid Pool by Convection

The model used for the heat flow from convection was developed by considering the surface of the pool as a flat plate over the ground as shown in Figure 2. Moreover it takes into account the prospects of turbulent or laminar boundary layers using dimensionless numbers [6].

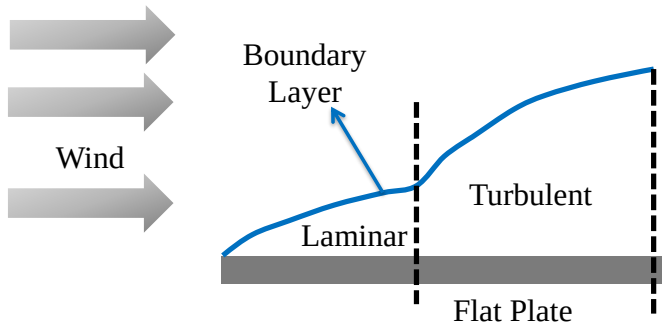

Figure 2: Formation of boundary layer over the flat plate due to wind

$$Q_{Conv} = \frac{\lambda_a \, N_u \, \pi \; r^2 \, (T_a - T)}{1000 \, L} \qquad 2$$

where,

λ_a Thermal conductivity of air, W m^{-1} K^{-1}

N_u Nusselt number, dimensionless

T_a Atmospheric temperature, K

L Diameter of the pool, m

Q_{conv} Heat flow rate from conduction, kW

The thermal conductivity of air is a function of the temperature. The air temperature near the surface of the pool will be lower than the surroundings temperature due to the cold vapors. The properties of air are usually not calculated at the surroundings temperature but at an average temperature, $(T_a + T)/2$. The Nusselt number, a dimensionless number expressing the ratio of convective heat transfer to conductive heat transfer, will vary with the type of boundary layer above the liquid pool [5].

Particularly for cryogens, In case of laminar flow, Re < 320000

$$N_u = 0.664 \; P_r^{1/3} \, R_e^{1/2} \qquad 3$$

where,

P_r Prandtl number, dimensionless

R_e Reynold number, dimensionless

In case of Turbulent flow, Re > 320000

$$N_u = 0.037\, P_r^{1/3}\, [R_e^{0.8} - 15200] \quad (4)$$

and,

$$P_r = (C_{Pa}\, \mu_a)/\lambda_a \quad (5)$$

$$R_e = (U_{10}\, \rho_a\, L)/\mu_a \quad (6)$$

where,

C_{Pa} Atmospheric specific heat capacity J kg^{-1} K^{-1}

μ_a Atmospheric dynamic viscosity, kg m^{-1} s^{-1}

ρ_a Density of air, kg m^{-3}

U_{10} Velocity of air at 10 m height, m s^{-1}

The specific heat capacity, dynamic viscosity and density of air in the boundary layer are calculated as function of average temperature of atmosphere and cryogen pool. Equation 6 refers to the wind velocity at 10 m height that can be obtained by Log Wind Profile or Power Law. The latter is used when surface roughness or atmospheric stability are unknown. The surface roughness length depends upon the type of area (congested or uncongested)[7]. Wind profile is naturally logarithmic. Log Wind Profile provides the best estimate of wind speed at different heights [8].

$$\check{U} = \frac{\check{U}_1 \log(z_1/z_0)}{\log(z/z_0)} \quad (7)$$

where,

$\check{U}$	Velocity at the required height, m^{-1}
$\check{U}_1$	Known velocity at height z_1, m s^{-1}
z_1	Height at which $\check{U}_1$ is calculated, m
z	Height at which $\check{U}$ is required, m
z_0	Surface roughness length, m

If the heat provided to the pool (by conduction, convection or radiation) is smaller than the heat taken by phase change, the temperature of the liquid pool drops down below its boiling point and the boiling regime switches into the evaporation. The attention taken towards evaporation mode is important because, like the heat flux provided to the pool due to the convection, the heat flux taken from the pool due to evaporation is also a function of the wind speed. Therefore, a shift from boiling to evaporation may happen at a particular wind speed. The change of the temperature of liquid pool is a good indication of the change of vaporization mechanism as evaporation is a cooling phenomenon. If the cryogenic liquid is spilled below the boiling point and sufficient heat is provided to the pool it will take some time to reach the boiling temperature. As long as the pool is in the boiling regime the temperature of the pool will stay at the boiling point. However, as soon as the heat provided to the pool becomes insufficient, the pool enters the evaporation regime again and pool temperature will start to drop down as shown in Figure 3.

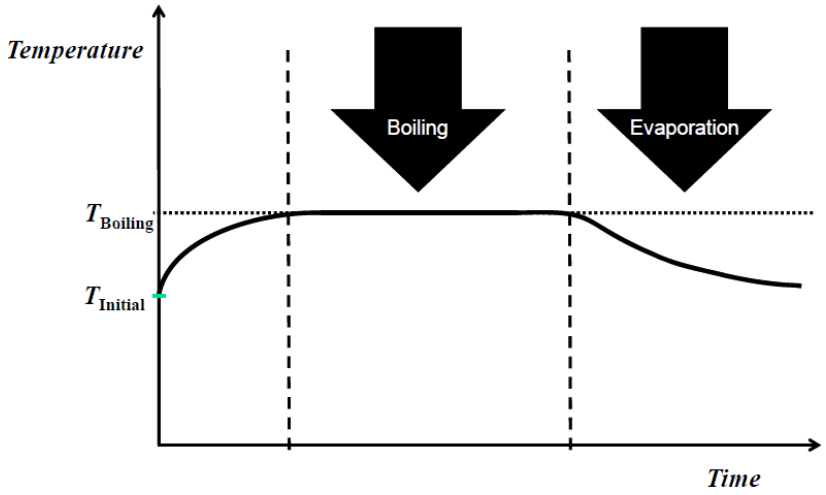

Figure 3: Variation in heat transfer modes with change in temperature

3.3 Heat Flow Rate from the Liquid Pool by Evaporation

Evaporation is an endothermic process which uses the liquid pool itself as a heat reservoir. It is a mass transfer phenomenon that occurs when the concentration of the substance of concern at the surface of the liquid (vapor pressure of liquid) is higher than its concentration in the surrounding (partial pressure in the atmosphere) and the temperature of the liquid is lower than its boiling point. Evaporation occurs at the surface and highly depends upon the wind speed. The higher the wind speed, the more vapors will be removed from the layer above the liquid surface allowing more molecules to shift from liquid to vapor phase.

Webber and Witlox suggested to adopt the non-unified treatment for the cryogenic pool in which the evaporation and boiling regimes can be distinguished based on the temperature of the pool [9]. Several models exist to date to predict the evaporation regime [5,10–14]. The driving force of evaporation is the difference between the vapor

pressure of the liquid at the liquid surface and its partial pressure in the surroundings. In general, all of the existing models can be classified into two different categories, distinguished by the term accounting for the driving force, which are namely linear or logarithmic. Earlier models were based on the linear driving force [10,12] which were replaced later by opting logarithmic driving force [5,11]. The latest models [13,14] adopt the linear driving force because of the limitations associated with the use of logarithmic driving force. The difference between the evaporation models adopting similar driving force is mainly because of the selection of different correlations for the mass transfer coefficient.

A general equation for evaporation adopting a linear driving force is given by

$$E_{vap} = \frac{\pi\, r^2\, K_m\, M_w}{R\, T} P_v \qquad 8$$

Film theory, for high mass transfer rates, suggested a correction term for the mass transfer coefficient (details will be discussed later) to formulate the evaporation model adopting the logarithmic driving force [11], may be written as follows

$$E_{vap} = \frac{\pi\, r^2\, K_m\, M_w}{R\, T} P_a \ln\frac{P_a}{P_a - P_v} \qquad 9$$

and the heat flow rate due to evaporation will be

$$Q_{evap} = E_{vap}\, H_V \qquad 10$$

where,

Q_{evap} Heat flow rate from evaporation, W

E_{vap} Evaporation rate, kg s^{-1}

r	Radius of the pool, m
K_m	Mass transfer coefficient, m s^{-1}
M_w	Molecular weight of spilled liquid, kg $kmol^{-1}$
H_v	Heat of vaporization of spilled liquid, J kg^{-1}
P_v	Saturated vapor pressure of spilled liquid, Pa
R	Universal gas constant, J K^{-1} $kmol^{-1}$
T	Temperature of the pool, K
P_a	Atmospheric pressure, Pa

This section will give insight to the theoretical background in order to bring an understanding of the development procedure of the models being used for the source term. It will include the assumptions, verification, and validation of the models to assess the applicability of each model for boiling or non-boiling pools. It will also identify the most effective model in terms of computation time and accuracy.

3.3.1 Linear Evaporation Model by Mackay, D. & Matsugu, R.,1973 for Non-Boiling Liquids

The presence of two or more components in the liquid brings complication to mass transfer due to phase resistance. The lighter components will vaporize during the early stage of pool vaporization which will leave behind the heavier components, restricting the mass transfer phenomena. As long as only single component liquids are considered there will not be any liquid phase resistance associated with the evaporation [10]. Mackay and Matsugu's model for the evaporation takes into account only one

component and the vaporization rate from evaporation is the same as given by equation 8. The mass transfer coefficient is a function of transportation conditions above the pool, diffusivity coefficient, and the pool radius. It is given by

$$K_m = C\ U_{10}{}^{d} L^{e} \qquad 11$$

where,

C Constant obtained from experimental data, dimensionless

e Power of diameter of the pool, dimensionless

d Power of velocity of air, dimensionless

Experiments were performed over water, cumene and gasoline to get the value of C. The temperature of surrounding was regulated from 278 K to 303 K. The wind speed during the experiment was varied from 0 m s^{-1} to 6.7 m s^{-1} and the air temperature was varied from 5°C to 30°C. Two different sites were chose to perform the experiments. Evaporation of water was carried out on the roof of University of Toronto, Chemical Engineering Department and hydrocarbons (cumene and gasoline) were tested at Toronto Harbour near Eastern Channel of Toronto Island. Atmospheric data was provided by Toronto Island Airport.

Wooden rectangular evaporation pans of different sizes (4×4 ft. and 8×4 ft. with 0.75 inch depth) with epoxy resin coated base were used for experiments. The rate of evaporation for water was measured by calculating the rate of flow of water into the pan required to maintain a constant level. For gasoline, due of the constantly changing composition, the volume in the pan was recorded manually. The position of the pan was interchanged to make sure that there is no effect of a specific position on the evaporation

rate. Evaporation rate obtained from the experiment for different sizes of the pool is shown in Figure 4. Mackay and Matsugu suggested *e* value of -0.11 based on the experimental results.

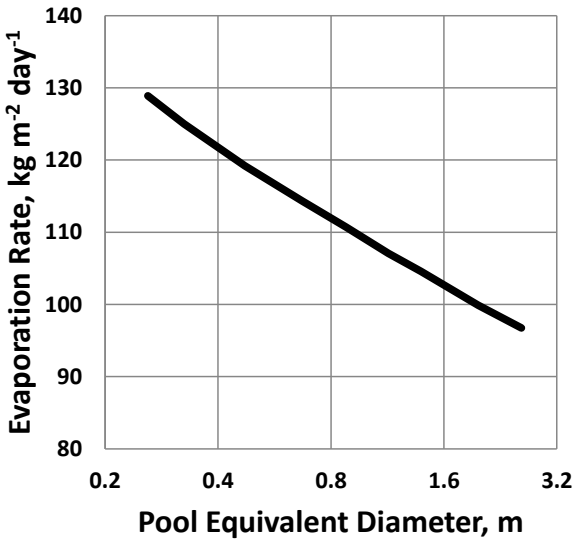

Figure 4: Effect of pool size on evaporation rate [10]

Earlier before Mackay and Matsugu, Sutton did important work in development of models for evaporation in the turbulent atmosphere. For the constant *d* value, Mackay and Matsugu relied on Sutton's work based on the efforts of Himus and Hine [15,16]. Himus and Hine did experiments in the wind tunnel using 25 gm water in evaporation dishes (1 ft. by 9 inch) and measured the mass loss as a function of wind speed.

Sutton developed equation 12 by using Von Karman similarity Principle

$$Evaporation\ rate \propto \check{U}_m^{\frac{2-n}{2+n}} \qquad 12$$

where,

$\check{U}_m$ Mean velocity of air, m s^{-1}

n Function of ground roughness and temperature profile, dimensionless

Considering no thermal effects and a turbulent medium, for a wide range of Reynolds Number, the variation in the average wind velocity as a function of height is given by [15],

$$\check{U} = \check{U}_1 \left(\frac{z}{z_1}\right)^{\frac{1}{7}} \quad 13$$

Sutton showed the variation in the wind velocity as a function of height, given by

$$\check{U} = \check{U}_1 \left(\frac{z}{z_1}\right)^{\frac{n}{2-n}} \quad 14$$

Comparing equation 13 and 14 will give,

$$n = \frac{1}{4}$$

Substituting *n* in equation 12 will give,

$$Evaporation\ rate \propto \check{U}_m^{\frac{7}{9}} \left(= \check{U}_m^{0.78}\right) \quad 15$$

Mackay and Matsugu agreed to this calculation and opted constant *d* value of 0.78. The mass transfer coefficient given by equation 11 can be written as,

$$K_m = C\ {U_{10}}^{0.78} L^{-0.11} \quad 16$$

The *C* value of 0.015 fits the experimental data obtained from the evaporation of cumene. This value is exclusively for cumene. For other substances, the authors suggested to opt $0.0292\ S_c^{-0.67}$ for estimation of *C* value. The term was proposed by

comparing the results with Fitzgerald model [17]. The verification was done for water evaporating in a 4 ft. tray at a surroundings temperature of 20°C and an average wind speed of 10 miles day^{-1}. The difference between the evaporation rate of water from Fitzgeral's model and Mackay and Matsugu's model, opting $0.0292\,S_c^{-0.67}$ for the estimation of *C*, was 0.17 inch per day. The authors stated it as good agreement and proposed $0.0292\,S_c^{-0.67}$ for the estimation of *C* value for all other substances other than cumene. Therefore, equation 16 can be written as

$$K_m = 0.0292\,S_c^{-0.67}\,{U_{10}}^{0.78}L^{-0.11} \qquad 17$$

and,

$$S_c = \mu_a/\rho_a D_{ac} \qquad 18$$

where,

S_c Schmidt number, dimensionless

D_{ac} Diffusion coefficient, m^2 s^{-1}

Diffusion coefficient can be calculated from the Chapman Enskog equation for binary mixtures [18].

$$D_{ac} = \frac{0.0018583\sqrt{T_m^3\left(\frac{1}{M_A}+\frac{1}{M_B}\right)}}{10000\,P_a\,\sigma_{AB}^2\,\Omega_{D_{ac}}} \qquad 19$$

where,

T_m Average temperature at which diffusion coefficient is measured, K

M_A Molecular weight of species 1, kg kmol^{-1}

M_B Molecular weight of species 2, kg kmol^{-1}

σ_{AB} Collision diameter, Å

$\Omega_{D_{ac}}$ Collision integral of diffusion, dimensionless

All of these values can be combined in equation 8 to calculate the vaporization rate due to evaporation, given by

$$E_{vap} = \frac{0.0292\,\pi\,r^2\,S_c^{-0.67}\,{U_{10}}^{0.78}\,L^{-0.11}\,M_w\,P_v}{R\,T} \qquad 20$$

3.3.2 Logarithmic Evaporation Model by Opschoor, G., 1979 for Non-Boiling Liquids

The author has discussed two theories, namely film theory and laminar boundary layer theory, to elaborate linear evaporation driving force given by equation 8. The theories led to the formation of a correlation that deals with the logarithmic driving force for evaporation of non-boiling liquids, as given by equation 9. Furthermore, a mass transfer coefficient was suggested by the author.

3.3.2.1 Laminar Boundary Layer Theory

The laminar boundary layer theory has been stated to be more accurate than the film theory but it can only be applied where the flow of air above the liquid pool is laminar. For this reason, the applicability of this theory is limited to very small sizes, not greater than a few centimeters. Therefore, the author focused more on the film theory.

3.3.2.2 Film Theory

The theory suggests that as the vapor pressure of the evaporating substance increase, the mass transport (evaporation) also increases. At high mass transports (higher than a limit to be determined), the mass transfer coefficient is not the only parameter to be considered for evaporation rate but the mass flow due to high pressure gradient, between the pool and the atmosphere surrounding it, should also be taken into account [11]. A correction factor for the mass transfer coefficient was proposed in case of high mass transports [19], given by.

$$K' = \frac{K_m\,(P_a - P_v)}{P_v} \ln\left[1 + \frac{P_v}{P_a - P_v}\right] \qquad 21$$

where,

K' Corrected mass transfer coefficient, m s^{-1}

The correction factor enables the evaporation model to be used for both high and low mass transport rates. Introducing K' instead of K_m in equation 8 will lead to

$$E_{vap} = \frac{\pi\, r^2\, K_m\, M_w}{R\, T} (P_a - P_v)\, \ln\left[\frac{P_a}{P_a - P_v}\right] \qquad 22$$

At low vapor pressures, P_V will be negligible and equation 22 will reduce to

$$E_{vap} = \frac{\pi\, r^2\, K_m\, M_w}{R\, T} P_a\, \ln\left[\frac{P_a}{P_a - P_v}\right] \qquad 23$$

Equation 23 formulated the basis for models adopting the logarithmic driving force to calculate the evaporation rate. To calculate the mass transfer coefficient, the author estimated the *C* value from an acrylonitrile experiment published by the

Commission for the Prevention of Disasters by Dangerous Substances, Netherlands [20]. Brief data of the experiment has been tabulated in Table 2.

Table 2: Mass transfer coefficients for evaporation of acrylonitrile for calculating *C*

K_m, m s^{-1}	C x 10^{-3}, $m^{0.44}$ $s^{-0.22}$	U_{10}, m s^{-1}	T, K
0.013	3.9	9	282
0.011	3.2	9	282
0.009	2.7	9	282
0.008	2.3	9	282
0.009	2.6	9	282

The author has suggested the best estimate of mass transfer coefficient, based on the experimental data, to be 0.0026. Therefore the mass transfer coefficient can be written as

$$K_m = 0.0026\, U_{10}^{0.78}\, L^{-0.11} \qquad 24$$

Substituting the mass transfer coefficient in equation 23 will give

$$E_{vap} = \frac{0.0026\, \pi\, r^2\, U_{10}^{0.78}\, L^{-0.11}\, M_w}{R\, T}\, P_a\, \ln\left[\frac{P_a}{P_a - P_v}\right] \qquad 25$$

Opschoor's model was neither validated nor verified. The author stated that investigation is being carried out for the validation of the model against experiments using toluene in a wind tunnel. The author further stated that the provisional experimental results corresponded well with the calculated results as per personal communication with Colenbrander, G.W. but no results were published. However, the author mentioned that the experiments were carried out for vapor pressure up to

90,000 Pa and therefore the model shouldn't be used for liquids with vapor pressure above 90,000 Pa.

3.3.3 Linear Evaporation Model by Reed, M., 1989 for Non-Boiling Liquids

The model by Reed, M. is based on the work of Mackay and Matsugu with the only difference of the molecular weight term [12]. The author adopted the mass weighted average molecular weight of the substance that forms the pool referenced to molecular weight of air, $\sqrt{M_c + 29/M_c}$. The evaporation rate formulated by Reed is given as

$$E_{vap} = \frac{0.029\,\pi\,r^2\,S_c^{-0.67}\,{U_{10}}^{0.78}\,L^{-0.11}\,P_v\,\sqrt{M_c + 29/M_c}}{R\,T} \qquad 26$$

Subsequently, the heat flow rate due to evaporation will be given by the general equation10. Unfortunately, **no validation or details on why to opt for mass weighted average molecular weight has been provided by the author**.

3.3.4 Logarithmic Evaporation Model PVAP,2006 for Boiling and Non-Boiling Liquids

DNV's (Det Norske Veritas, a Norwegian society organized in 1864 to safeguard life, property and environment) industrial hazard analysis software, PHAST, has developed the model PVAP. A modification to Mackay and Matsugu's model was the introduction of the logarithmic term associated with the vapor pressure which is considered to be the driving force in the particular case of evaporation [5]. The model under discussion closely resembles with the one developed by Opschoor. The difference

lays under the mass transfer coefficient and to be more precise, in the constant *C* value. Association of PVAP model with the commercial software PHAST 6.7 has established a special interest in understanding of model. In other words, reliability of the model will affirm the reliability of the software.

The mass transfer coefficient for PVAP is estimated by

$$K_m = 0.015\, U_1^{0.25}\, S_c^{0.67}\, L^{-0.11} \qquad 27$$

The constant value of 0.015 was chosen for *C* based on the experimental data of Kawamura and Mackay [21]. The difference between the constant opted by Mackay and Matsugu, and PVAP is mainly because Mackay and Matsugu's model monitors evaporation with linear driving force whereas PVAP handles evaporation with logarithmic driving force. Therefore equation 9 can be written as

$$E_{vap} = \frac{0.014\, \pi\, r^{1.89} S_c^{-0.67}\, {U_1}^{0.25} M_w}{R\, T}\, P_a\, ln\left(\frac{P_a}{P_a - P_v}\right) \qquad 28$$

The adoption of the logarithmic factor in the equation comes from the earlier work on the film theory [22]. The theory does not only take into account the diffusion of a component through other but it also considers the mass transport of liquid into vapor phase. A correlation was derived for the steady-state diffusion in the binary system where only one component diffuses through the other and a logarithmic factor for mole fraction, just above the pool, was also introduced in the mass transfer coefficient to account for the mass transport. The factor was named as 'film pressure factor'. The same factor was used by Bird [18] to derive correlation for the diffusion through a stagnant gas.

The film pressure factor was discussed by Brighton [23] and Webber [24]. At equilibrium, the evaporation rate should be function of the following

$$E_{vap} \propto A\ V_c\ S_c U_*\ f(x) \tag{29}$$

where,

A Area of pool, m^2

V_c Vapor concentration at the surface, kg m^{-3}

U_* Atmospheric friction velocity, m s^{-1}

$f(x)$ Function of the mole fraction of vapor at pool surface, dimensionless

This function of the mole fraction of the vapor at the pool surface is the same as mentioned by Sherwood as film pressure factor and has been further elaborated as,

$$f(x) = \frac{1}{x}\ ln\frac{1}{(1-x)} \tag{30}$$

$$x = \frac{P_v}{P_a} \tag{31}$$

The correction factor applies to the high vapor pressures because near the boiling point convective mass transfer can become more dominant than the diffusion mass transfer. The correction factor will better estimate the mass transfer coefficient by taking into account both, diffusion and bulk mass transfer.

for, $x \ll 1$

$$f(x) \sim 1$$

and for, $x \to 1$

$$f(x) \to \infty$$

This PVAP model shows irregular behavior when used for cryogenic liquid as the boiling point is reached very quickly followed by the loss of containment. Equations 29, 30 and 31 suggest that the higher the temperature of the pool, the higher will be the vapor pressure and the vaporization rate. Near the boiling point the vaporization rate will tend to infinity which may cause computational errors.

PVAP was validated against the experiments performed by Kawamura and Mackay. The experiments were conducted in Woodbridge Ontario using a number of chemicals, namely toluene, cyclohexane, n-hexane, methanol, pentane, dichloromethane and tri-chloro-fluro-methane (freon-11), in flat circular pans under different weather conditions to study the effect of evaporation rate. Experiments were performed during day time and atmospheric data was obtained from the weather office. Two sets of experiments were conducted. The 1st set of experiments was carried out to study the evaporation rate of the various chemicals by eliminating the conduction heat flux from the ground whereas the 2nd set of experiments took conduction heat flux into account as well [21].

In the first set, the sizes of the evaporation pans used in the experiment were 0.61 m and 0.91 m in diameter with a depth of 0.05 m. Styrofoam boards were used under the evaporation pans to avoid conduction from ground. The pan size chosen for a particular experiment was based on the volatility of the chemical to be used in the experiment and the weather conditions. Moreover the pans were painted with black color epoxy from inside to make sure perfect insulation.

A 6 L glass reservoir was filled with the chemical at ambient temperature. A glass tube was attached to it from one end and the other end of the glass tube was in the evaporation pan. The purpose was to maintain a constant level in the evaporation pan. On the basis of the amount of chemical lost from the reservoir, over a specific period of time, the evaporation rate was directly measured. The apparatus used for this purpose is shown in Figure 5.

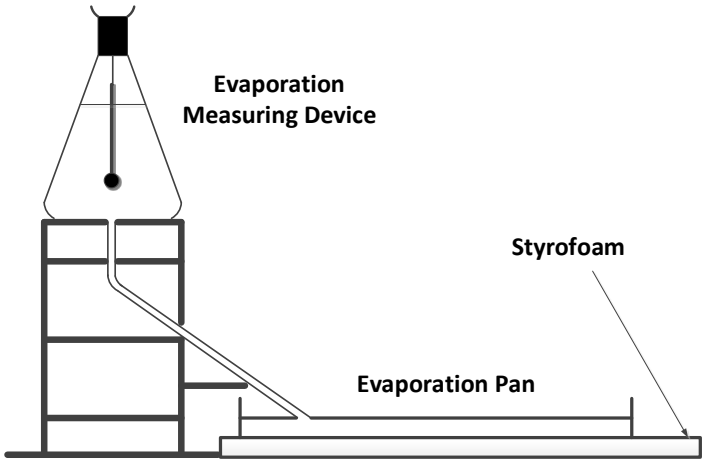

Figure 5: Apparatus to measure evaporation without conduction [21]

The second set of experiments was performed using 0.46 m diameter pan of with a depth of 0.102 m. The purpose of the experiment was to include the effect of conduction along with evaporation. To achieve that, pan was filled with sand (0.05 mm to 1 mm diameter particle size) to a depth of 0.05 m and buried into the ground in a way that the level of the sand remains just above the level of the ground. To eliminate the chance of sorption of the material on sand, the sand was saturated with water before the experiment. Experiment was performed with Toluene, cyclohexane, n-hexane,

dichloromethane and tri-chloro-fluro-methane (freon-11). The chemical in the pan was allowed to evaporate till, either the level of material inside the pan drops below 1 cm or the experiment runs for an excessively long duration. The evaporation rate was measured by the decrease in volume of the reservoir. The wind speed was measured by cup-counter anemometer. It was later adjusted to 10 m height by using the wind profile (power law or log wind profile) and surface roughness factor.

A steady state was defined as, the time after which the change of temperature of the chemical is not more than 2 °C over 5 min. Data after steady state is averaged over a time span of 30 min to 60 min [21]. The results of the experiments are shown in Table 3. PVAP was validated for the same set of data. The evaporation rate along with the deviation between the experimentally measured evaporation rate and the predicted evaporation rate by PVAP are shown in Table 4.

The results show an over prediction of evaporation rate by PVAP with an average absolute percentage deviation of 52 % [5]. The results seem to indicate that the lower the wind speed the more conservative is the model. It has also been mentioned in the PVAP theory document [5] that the validation was also carried out by adopting the original Mackay and Matsugu's model for the evaporation. The validation results are shown in Table 5.

The average absolute percentage deviation by adopting Mackay and Matsugu's model for evaporation is 23% which is lower than the average absolute percentage deviation observed for PVAP. It has been suggested in the PVAP theory document to revert to the original linear model proposed by Mackay and Matsugu.

Table 3: Experimental results of Kawamura and Mackay [21]

Test No.	**KM18**	**KM19**	**KM20**	**KM21**	**KM22**	**KM23**
Substance	Toluene	Cyclo-Hexane	n-Hexane	n-Pentane	n-Pentane	Freon 11
Spill Mass, kg	3.45	3.08	2.61	4.35	2.49	10.24
Release Temp, K	298	302	300	296	298	295
Solar Rad. W m^{-2}	872	894	728	647	861	853
Atm. Temp, K	298	302	300	296	298	304
Wind Speed, m s^{-1}	2.65	3.14	1.59	4.94	5.42	1.17
Surface Temp, K	298	302	300	296	298	304

Furthermore, PVAP is not valid for materials having a saturated vapor pressure up to 90,000 Pa [5]. As an example, for10 tons of methane spilled at a temperature of 108 K, the saturated vapor pressure may range from 74100 to 101325 Pa during the course of vaporization [25]. So, at a particular time, the saturated vapor pressure may go beyond the maximum allowable limit of vapor pressure to use PVAP.

Table 4: Validation of PVAP [5]

Test No.	KM18	KM19	KM20	KM21	KM22	KM23
Measured Evap. Rate x10^3, kg s^{-1}	0.1795	0.4338	0.3357	1.062	1.2514	1.6104
Predicted Evap. Rate x10^3, kg s^{-1}	0.2677	0.6093	0.6449	1.2705	1.5773	2.9718
Deviation, %	-49	-40	-92	-20	-26	-85

Table 5: Validation by adopting Mackay and Matsugu's Model [5]

Test No.	KM18	KM19	KM20	KM21	KM22	KM23
Measured Evap. Rate x10^3, kg s^{-1}	0.1795	0.4338	0.3357	1.062	1.2514	1.6104
Predicted Evap. Rate x10^3, kg s^{-1}	0.2302	0.5360	0.4619	1.17	1.4908	1.9454
Deviation, %	-28	-24	-38	-10	-19	-21

3.3.5 Linear Evaporation Model EFFECTS,2009 for Boiling and Non-Boiling Liquids

EFFECTS model adopts the linear approach to evaporation. It differs from Mackay and Matsugu's model in terms of the constant for the mass transfer coefficient. The mass transfer coefficient for EFFECTS model is given by

$$K_m = 0.004786\, S_c^{-0.67}\, {U_{10}}^{0.78} L^{-0.11} \qquad 32$$

The vaporization and heat flow rates can be determined by using the mass transfer coefficient in equation 8 and 10 respectively. It has been claimed by the author that the transition between the boiling and non-boiling liquids is very smooth using EFFECTS. Moreover, experiments with ammonia (boiling point 240 K) showed that evaporative cooling may cause the temperature of ammonia to decline, as low as 198 K [13]. Unfortunately, no discussion on the experiment and results was made by the authors.

EFFECTS was not validated against experimental data was verified with GASP (Gas Accumulation over Spreading Pools is a model developed by Webber [26] to account for the pool spreading of an evaporating or boiling liquid) and PHAST 6.0 [27]. An instantaneous spill of 10 tons of LNG in a bund of 5 m radius was considered. It can be seen from Figure 6 that the three models show different results although EFFECTS and GASP are relatively in accordance with each after 1000 s whereas PHAST 6.0 shows a comparatively different behavior.

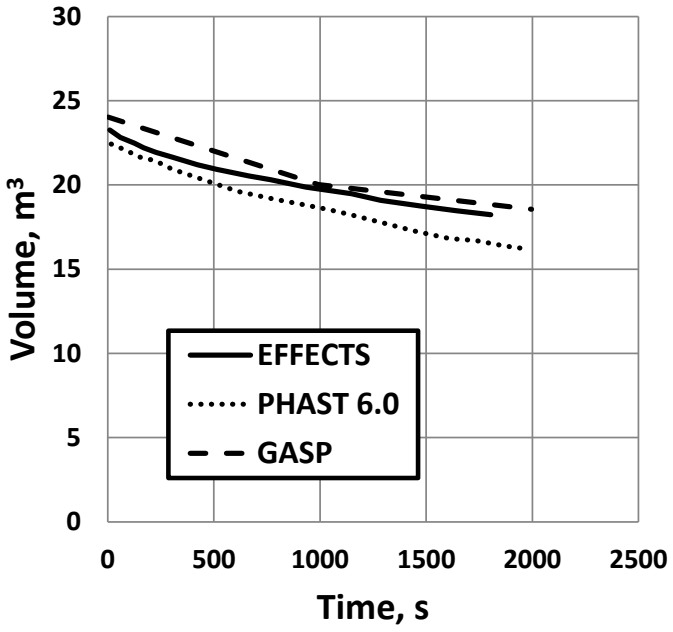

Figure 6: Verification of EFFECTS against PHAST 6.0 and GASP for pool volume [13]

From Figure 7, it can be seen that the pool temperature calculated by the three models shows different results. The predicted LNG pool temperature by EFFECTS model falls between the estimates obtained by PHAST 6.0 and GASP. PHAST 6.0 shows a drop in the temperature of the LNG pool after almost 500 s whereas EFFECTS predicts the decrease in temperature after 1000 s. The temperature of the LNG pool before complete vaporization is estimated to be -174°C, -164°C and -162°C by using PHAST 6.0, EFFECTS and GASP respectively. The complete vaporization of the LNG pool is observed earliest for PHAST 6.0 followed by EFFECTS and GASP respectively.

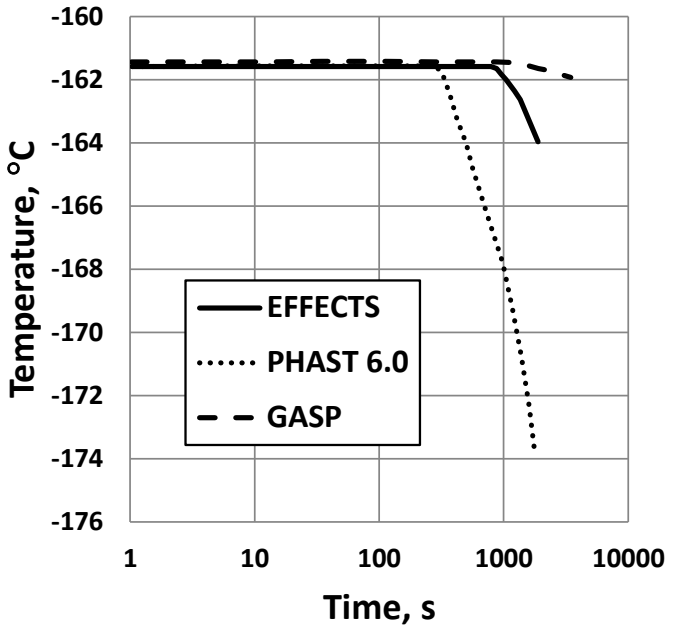

Figure 7: Verification of EFFECTS against PHAST 6.0 and GASP models for pool temperature [13]

3.3.6 Linear Evaporation Model PVAP-MC,2012 for Boiling and Non-Boiling Liquids

Based on the linear driving force for evaporation, PVAP-MC is the latest model for evaporation. The model is an extension to PHAST's PVAP and can be used to account for the mixture as pseudo component [14]. The mass transfer coefficient for PVAP-MC is given by

$$K_m = 0.005165\, U_{10}^{0.78}\, S_c^{-0.67}\, L^{-0.11} \qquad 33$$

Substituting in equation 8 with an additional term to account for the multicomponent

$$E_{vap} = \frac{0.004786\, \pi\, r^{1.89}\, S_c^{-0.67}\, {U_{10}}^{0.78} M_w\, X\, P_v}{R\, T} \qquad 34$$

where,

X Mole fraction of specific component in pool, dimensionless

For pure component, the equation will reduce to

$$E_{vap} = \frac{0.004786\,\pi\, r^{1.89}\, S_c^{-0.67}\, {U_{10}}^{0.78} M_w\, P_v}{R\, T} \quad (35)$$

PVAP-MC was verified against LPOOL, a model developed by Cavanaugh for modeling the spills of multicomponent liquids over land or water [28]. LPOOL was used by Shell to model the dispersion of vapors or gasses [29].

A constant spill of pure methane at a rate of 5 kg s^{-1} for 2 min was simulated, initially at its boiling point, with 1 m s^{-1} wind speed (measured at 10 m height). The temperature of the surroundings and the substrate was taken to be the same, 288 K. Solar radiation was neglected. Thermal properties and surface diffusivity were taken from LPOOL for consistency. Figure 8 shows that LPOOL and PVAP-MC are in agreement with each other. The calculated difference between the predictions by both of the models is of maximum 5% deviation.

The model was validated against the already published experimental data [21]. The scenario used to validate the PVAP-MC is described in Table 6 and the evaporation rate along with the deviation between the experimentally measured evaporation rate and the predicted evaporation rate by PVAP-MC are shown in Table 7. The average absolute percentage deviation between the estimate by the model and experimental measurement is 24.5 %. The deviation with a negative sign shows that the model was conservative as it predicted higher evaporation rate than the measurement.

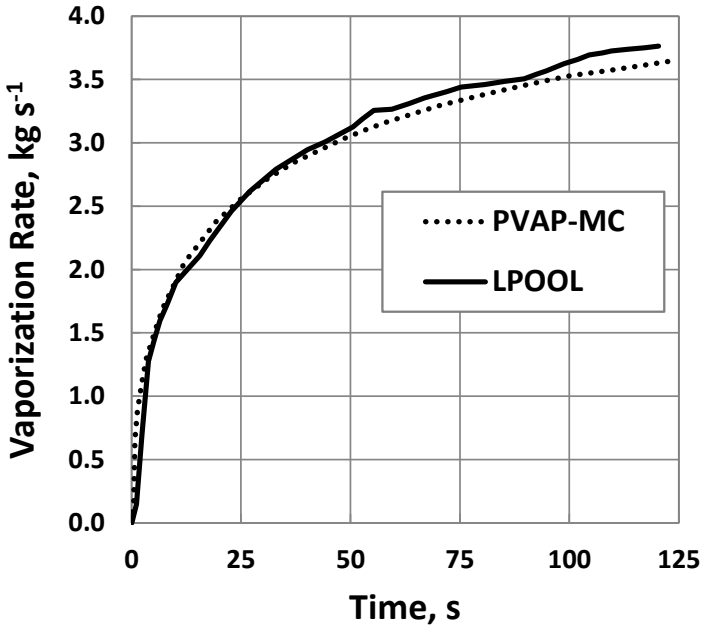

Figure 8: Comparison of PVAP-MC and LPOOL for methane pool vaporization [14]

Table 6: Validation scenario for PVAP-MC [14]

Spill	Instantaneous
Reference Height for Wind Speed, m s^{-1}	10
Bund Diameter, m	0.46
Type of Surface	Sand – user defined
Surface Roughness Factor	2.6
Thermal Conductivity, W m^{-1} K^{-1}	2.08
Thermal Diffusivity, m^2 s^{-1}	7 x 10^{-7}

Table 7: Validation of PVAP-MC [14]

Test No.	KM18	KM20	KM21	KM22
Measured Evap. Rate, kg m^{-2} h^{-1}	3.9	7.28	23	27.1
Predicted Evap. Rate, Kg m^{-2} h^{-1}	4.42	10.31	27.08	33.79
Deviation, %	-13	-42	-18	-25

3.4 Comparison of the Models

The equations giving the mass transfer coefficients used by models have been listed in two tables. Table 8 shows the mass transfer coefficients of the models adopting linear driving force whereas Table 9 shows the mass transfer coefficients of the models adopting the logarithmic driving force.

The constant value *C* for the mass transfer coefficient has changed over the years. Reed's evaporation model adopts the mass weighted average for the molecular weight of the evaporating liquid with respect to the molecular weight of air. Summary of the models on the basis of verification and validation has been provided in Figure 9. It can be seen that none of the models were validated against the cryogens. The current version of PHAST 6.7, hazard analysis software, adopts the model PVAP. The model predicts a drop in temperature for the cryogenic pool which suggests that the pool undergoes the evaporation regime. It is a question that cannot be answered without validation.

Table 8: Comparison of mass transfer coefficients with linear driving force

Model	Mass Transfer Coefficient, m s^{-1}
Mackay & Matsugu [10]	$0.0292\ U_{10}^{0.78} / S_c^{0.67}\ (2\,r)^{0.11}$
Reed [121]	$0.0292\ U_{10}^{0.78}\ \sqrt{M_c + 29/M_c} / S_c^{0.67}\ (2\,r)^{0.11}$
EFFECTS [13]	$0.004786\ U_{10}^{0.78} / S_c^{0.67}\ (2\,r)^{0.11}$
PVAP-MC [14]	$0.004786\ U_{10}^{0.78} / S_c^{0.67}\ (r)^{0.11}$

Table 9: Comparison of mass transfer coefficients with logarithmic driving force

Model	Mass Transfer Coefficient, m s^{-1}
Opschoor [11]	$0.0026\ U_{10}^{0.78}\ /\ (2r)^{0.11}$
PVAP [5]	$0.014\ U_1^{0.25} / S_c^{0.67}\ (r)^{0.11}$

As per the personal communication with Dr. Henk Witlox, overall SAFETI-NL project manager DNV software, the new version of PHAST, PHAST 7.0, will adopt the model PVAP-MC instead of PVAP. It has also been mentioned by Dr. Witlox that the model will be validated for cryogens but no time frame was provided. For accurate source term modeling, it is required to question the possibility of evaporation regime for the cryogenic liquids. It is also needed to analyze the computational efficiency and accuracy of the evaporation models.

[1] M_c term in general formula is excluded

MODEL	VERIFICATION	VALIDATION	COMMENTS
MACKAY AND MATSUGU, 1973	✗	✓	Validation with **water, cumene and gasoline**.
OPSCHOOR, 1979	✗	✗	Personal Communication.
REED, 1989	✗	✗	Not mentioned.
PVAP, 2006	✓	✓	Verification against GASP model. Validation with **Toluene, Cyclo-hexane, Hexane, Pentane and Freon**.
EFFECTS, 2009	✓	✗	Verified against GASP and PHAST.
PVAP-MC	✓	✓	Verification against LPOOL model. Validation with **Toluene, Hexane and Pentane**.

Figure 9: Summary of evaporation models

4. METHODOLOGY

The objective of current research is to investigate the likelihood of evaporation heat transfer, its interaction with convective heat transfer and its effect on the predicted dominating vaporization mechanism during the vaporization of a non-reactive cryogenic liquid spill. The research approach described in Figure 10 was developed accordingly..

A simulation tool was formulated using MATLAB software to perform the simulation of the pool vaporization by taking into account the effect of conduction, convection and evaporation heat flux. The tool was used to verify the existing evaporation models (cross-comparison of the results) and further perform their validation by comparison with experimental data.

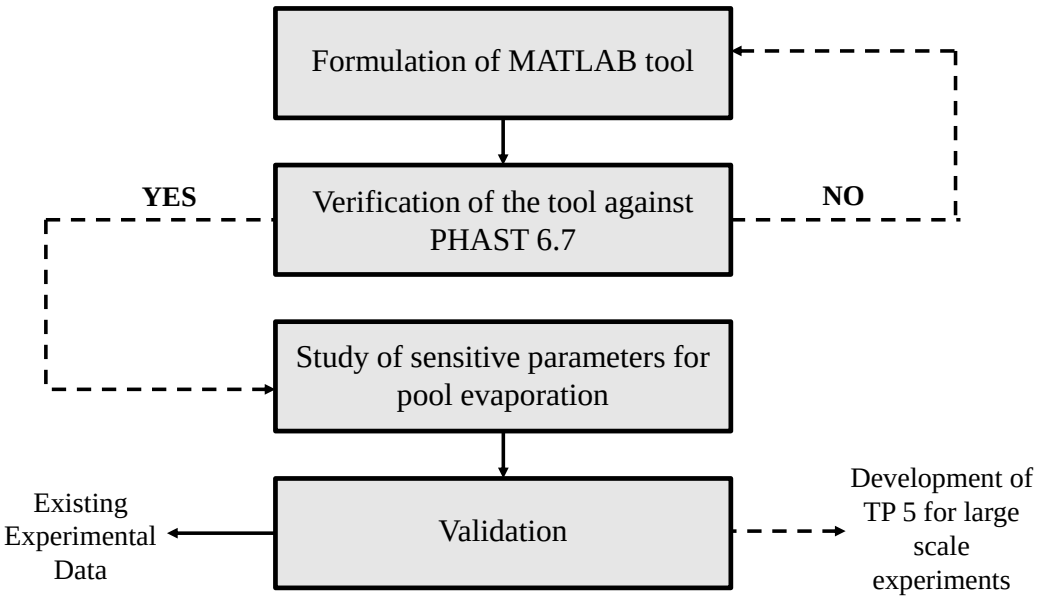

Figure 10: Approach developed to achieve the objectives of this work

4.1 Conservation of Energy and Mass

The developed MATLAB tool solves the energy and mass balance for the system shown in Figure 11.

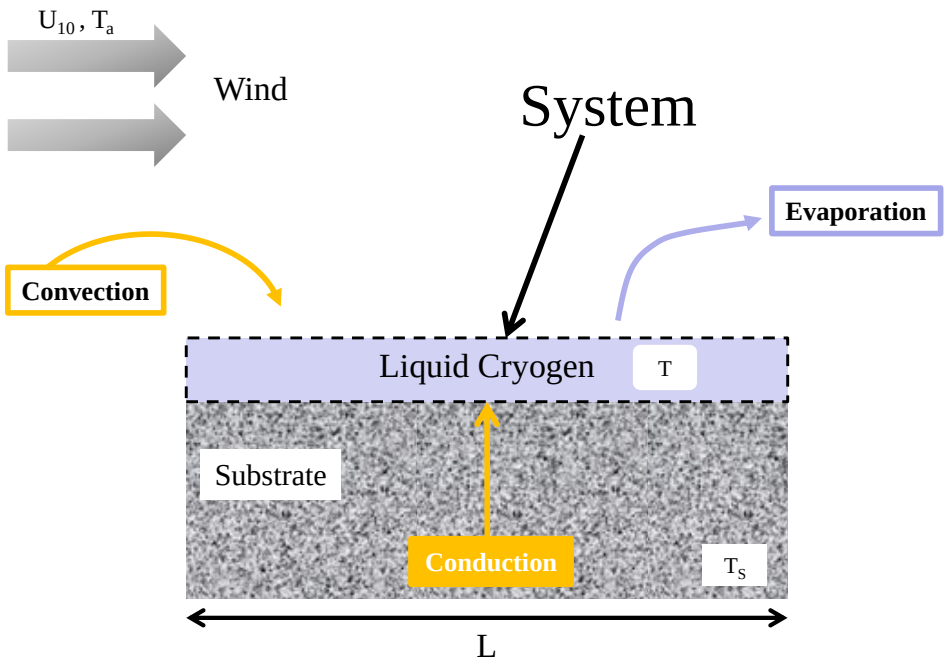

Figure 11: Defined system for mass and energy balance

In case of the loss of containment of non-reacting cryogenic liquids (i.e. LNG, LN_2), heat generation and heat consumption rates can be ignored in the energy balance as these terms are accounted for chemical reactions. The energy balance will be given by

$$\begin{aligned} &Energy\ Accumulation\ Rate \\ &= Rate\ of\ Energy\ Entering\ the\ System \\ &- Rate\ of\ Energy\ Leaving\ the\ System \end{aligned} \qquad 36$$

For the system at **boiling point**, the sensible heat of the pool does not change.

$$Energy\ Accumulation\ Rate, M\ C_P \frac{dT}{dt} = 0 \quad (37)$$

or, equation 37 can also be written as

$$\frac{dT}{dt} = 0 \quad (38)$$

where,

M Mass of the pool at particular time, kg

C_P Heat capacity of the liquid, kJ kg^{-1} K^{-1}

The energy entering the system at boiling point causes the phase change (liquid to vapor) and it is equal to the energy leaving the system.

$$Rate\ of\ Energy\ Leaving\ the\ System = \ Rate\ of\ Energy\ Entering\ the\ System$$

Mathematically it can be written as

$$Q_{boil} = \ Q_{cond} + Q_{conv} \quad (39)$$

where, Q_{boil} is the amount of heat released during the phase change, given by

$$Q_{boil} = \ M.H_V \quad (40)$$

therefore, equation 39 can be written as

$$M.H_V = \ Q_{cond} + Q_{conv} \quad (41)$$

The pool vaporization will decrease the mass of the pool. Therefore, equation 41 can be written as

$$\frac{dM}{dt} = \ - \frac{Q_{cond} + Q_{conv}}{H_V} \quad (42)$$

At **non-boiling** condition the energy balance, based on equation 36, can mathematically be expressed as

$$MC_P \frac{dT}{dt} = Q_{cond} + Q_{conv} - Q_{evap} \quad 43$$

To take into account the pool mass loss due to vaporization, equation 43 can be written as

$$\frac{dT}{dt} = \frac{Q_{cond} + Q_{conv} - Q_{evap}}{C_P \frac{dM}{dt}} \quad 44$$

where,

$$\frac{dM}{dt} = -\frac{Q_{evap}}{H_V} \quad 45$$

Equation 38 and 42 are used in the MATLAB program to account for the temperature and the vaporization rate of the boiling pool whereas equation 44 and 45 takes into account the same for the non-boiling pool.

4.2 Formulation of the MATLAB Tool

The MATLAB program was developed for the cryogenic liquid pool of known radius under given atmospheric conditions. A liquid (methane, nitrogen, hexane, cumene, and water) and a substrate (concrete, insulated concrete, dry soil, wet soil, polystyrene, wood, aluminum, ice, and water) are chosen for a particular simulation. The initial pool height is provided to the program for the estimation of the initial mass of the

liquid pool. Wind speed at 1 m height is used to develop a wind profile above the pool. However, for a particular simulation wind speed will be constant.

4.2.1 Properties of Substrate

The substrate properties (namely; thermal conductivity and thermal diffusivity) are function of the temperature of the substrate but to simplify the research approach these are taken as constant [5,30]. The constant values of thermal conductivity and thermal diffusivity for various substrates are listed in Table 1.

4.2.2 Properties of Liquid

The liquid properties (namely; specific heat capacity, latent heat of vaporization and saturated vapor pressure) are function of the pool temperature. Correlations were used for the calculation of temperature dependent properties of the liquid [25]. To establish the trend of these properties as a function of pool temperature, graphs are included in Appendix B.

4.2.3 Properties of Air

The air properties (namely; density, specific heat capacity, viscosity, and thermal conductivity) are function of air temperature and are calculated using correlations [25]. The air temperature near the surface of the pool will be lower than the ambient temperature due to the cold vapors of cryogenic liquid. The properties of air are usually not

calculated at the ambient temperature but at an average temperature of the liquid and the surroundings.

Liquid to air diffusion coefficient was calculated as a function of average temperature using equation 19 by Chapman Enskog [18]. The wind speed, as a function of surface roughness and height, was estimated using equation 7 for the logarithmic wind profile [7,8]. The exponential increase in the wind speed developed by the logarithmic wind profile can be seen from Figure 12.

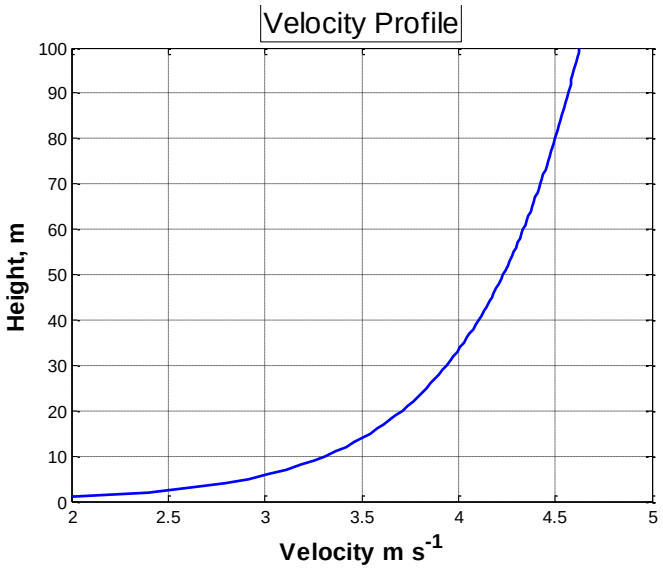

Figure 12: Logarithmic wind velocity profile

It is important to mention that the discussed fluid properties have a functional temperature range. If the temperature falls out of that limit the properties are no longer correct.

4.2.4 Algorithm

The developed algorithm for the MATLAB program is presented in Figure 13. A more detailed description is available in the Appendix A of this thesis.

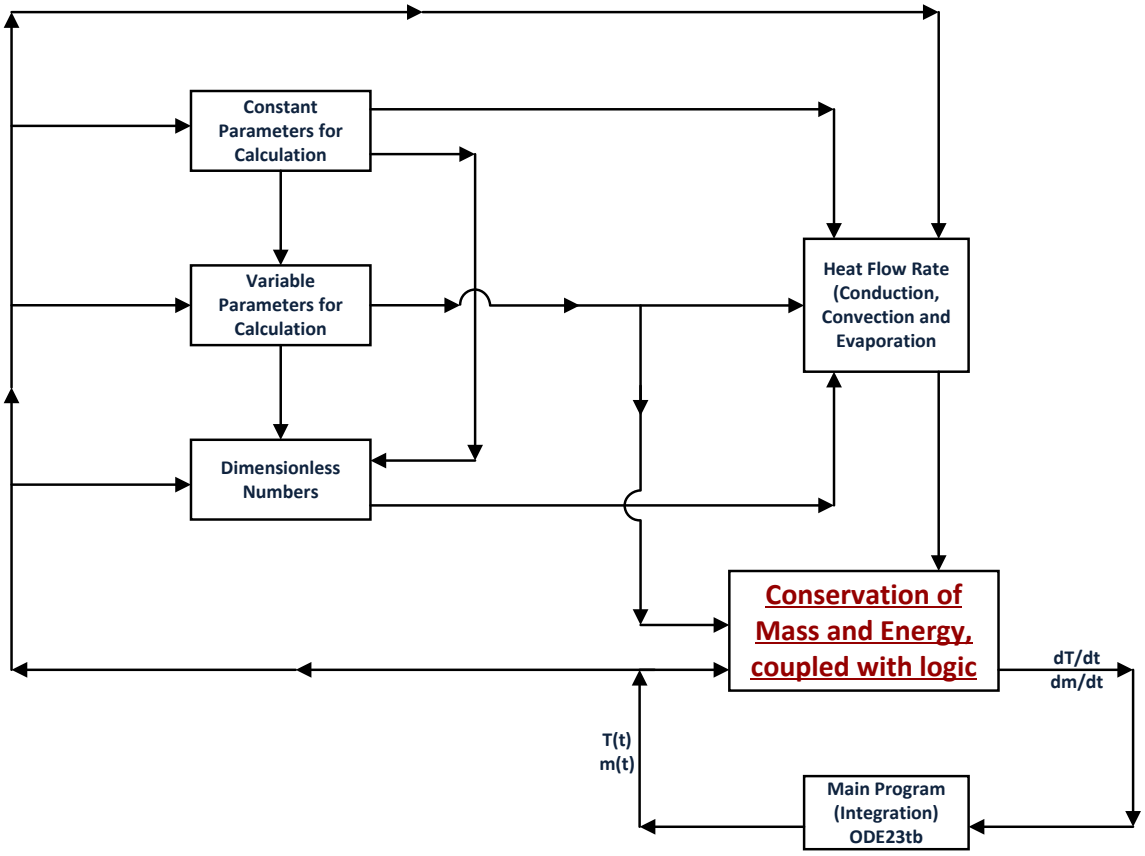

Figure 13: Algorithm for the MATLAB tool

- Constant parameters (e.g. wind speed, pool radius, and ambient temperature) are defined for a chosen scenario.
- Temperature dependent properties and wind profile are calculated.
- The constant parameters and variable properties are used for the calculation of dimensionless numbers (Nu, Pr, Re, Sc).

- The above mentioned parameters, liquid and air properties, and dimensionless numbers are used as inputs for the calculations of heat flow rates from conduction, convection and evaporation.
- The heat flow rates are used in the energy and mass balance equation of the liquid pool. However, these equations are different in boiling and evaporation regime, equation 38 and 42 for the boiling regime whereas equation 44 and 45 for the evaporation regime. The program required a logical expression to distinguish and shift between regimes.
- Two conditions can lead to the evaporation regime; either the temperature of the pool is lower than the boiling point of the liquid or the heat taken by evaporation heat flux is more than the heat provided by the conduction and convection heat flux, as shown in Figure 14. Otherwise, the pool is considered under the boiling regime with no change in the pool temperature.
- The two ODEs are passed on to the 'main program'. The solution of the equations (mass and temperature of the pool) is obtained by integrating the ODEs using solver ODE23tb. The initial pool temperature and the time of interest for the specified scenario are also defined in the main program.
- The solution obtained from the integration is used in the mass and energy balance, and also to calculate the temperature dependent properties for the next integration step. The integration will be performed until; the pool is completely vaporized or the time of interest is covered.

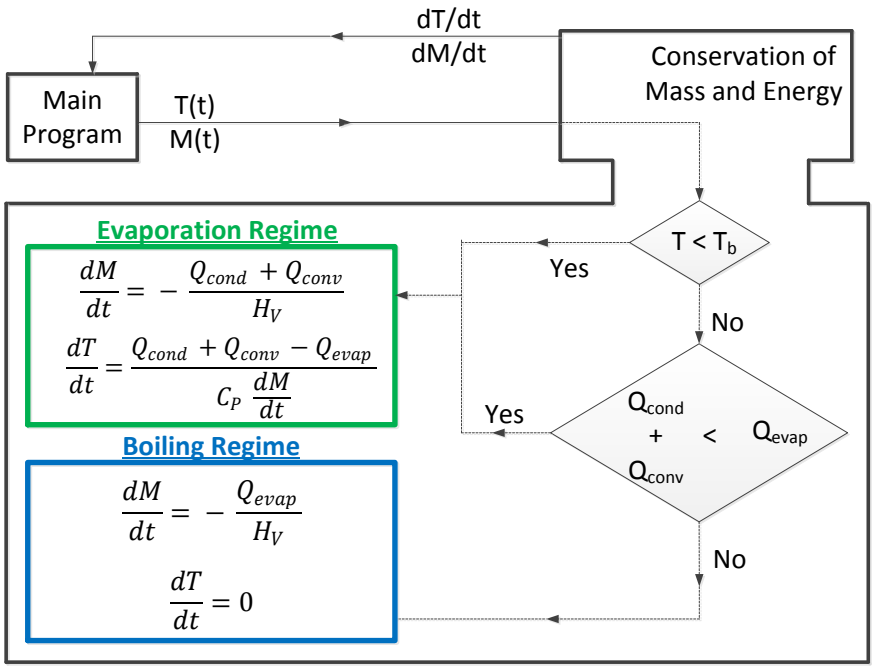

Figure 14: Algorithm of logical expressions

5. VERIFICATION AGAINST PHAST 6.7

It was required to verify the MATLAB program by cross-comparing its results against independent consequence modeling software to judge the quality of the results of the program. DNV's (Det Norske Veritas) industrial hazard analysis software, PHAST, was chosen for the verification of MATLAB tool. PVAP evaporation model was developed by PHAST. The model is being used in the current version of the software, PHAST 6.7.

Simulations were run for a 2.5 m radius liquid nitrogen pool on a concrete substrate under a wind speed 10 $m.s^{-1}$ at 10 m height. The ambient temperature was taken at 298 K. The substrate temperature is assumed to be initially at ambient temperature. The results for the variation of the pool temperature during the vaporization of the pool estimated by PHAST 6.7 and MATLAB program are compared in Figure 15. It can be seen that both the curves overlap each other till approximately 840 seconds. The verification provides confidence in the quality of the formulated MATLAB tool as it provides results similar to the commercial software PHAST 6.7 when used with the same evaporation model, PVAP.

After 840 seconds, the prediction of PHAST 6.7 software differs from the MATLAB tool. The difference comes from the fact that PHAST 6.7, unlike the MATLAB program, includes the pool decay model to take into account the decrease of pool radius as it reaches the minimum pool thickness (Figure 16). The MATLAB tool can be improved in future by including a valid model for the pool spreading and decay.

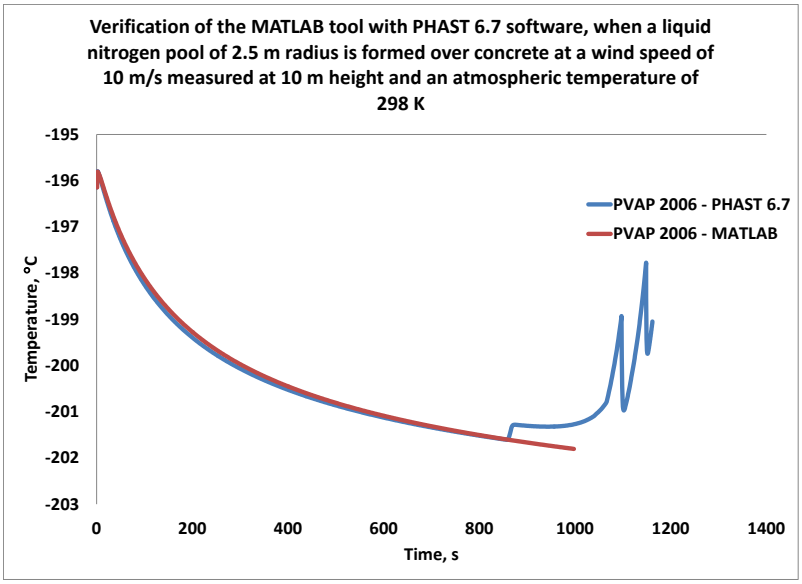

Figure 15: Verification of MATLAB tool with PHAST 6.7

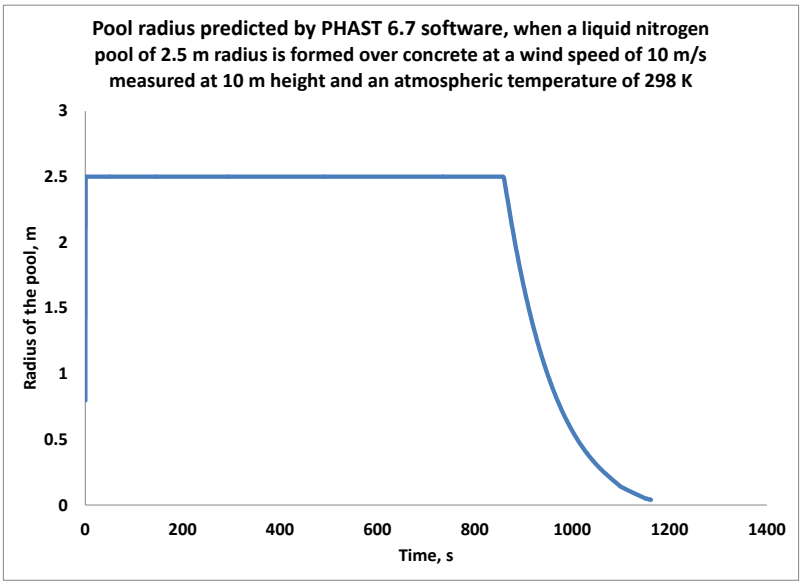

Figure 16: Radius of the pool using PHAST 6.7

6. RESULTS AND ANALYSIS

A comprehensive set of cryogenic liquid pool vaporization simulations using the MATLAB tool with the different evaporation models was performed to:

- Compare the evaporative heat flux predicted by the models particularly close to the boiling point;
- Observe the predicted change of vaporization regime (boiling to evaporation) for given evaporation models;
- Assess the sensitivity of the evaporation models to the cryogenic liquid pool dimensions, ambient temperature and the substrate.
- Cross-compare the dynamic of the vaporization of a given cryogenic pool when using different evaporation models;

For all the simulations radiative heat flux was neglected. Conductive heat flux was consistently modeled using the approach adapted from Carslaw and Jaeger which assumes the ideal contact of liquid and a uniform semi-infinite solid substrate (constant temperature of the substrate's surface at the liquid temperature – See section 3.1). Convective heat flux was modeled using the correlations for heat transfer over a flat plate as described in section 3.2.

The following models were used for the calculation of the evaporative heat flux: Mackay and Matsusgu's model, Opschoor's model, Reed's model, PVAP, EFFECTS, PVAP-MC [5,10–14].

6.1 Definition of a Base Case for the Study

A base case was defined to establish a scenario for the cross-comparison of the models. The summary of the characteristic parameters of the simulation is provided in Table 10.

Table 10: Parameters for the Base Case

Cryogenic liquid	Methane
Substrate	Concrete
Pool Radius (m)	2.50
Initial liquid pool temperature (K)	110.00
Liquid Boiling Point (K)	111.67
Wind speed at 10 m height (m s^{-1})	10.00
Wind profile	Logarithmic behavior (See section 3.2)
Ambient temperature (K)	298.00
Initial temperature of the substrate (K)	298.00
Initial height of the liquid pool (m)	0.10
Initial pool mass (kg)	1062.00

6.2 Comparison of the Predicted Evaporative Heat Flux

A very simple analysis of the predicted evaporative heat flux as a function of the pool temperature from the investigated models was performed. Figure 17 shows that the evaporation models tend to give similar results far from the boiling point. As the pool

temperature increases, the predicted evaporative heat flux consistently increases with all the models. As the pool temperature approaches the boiling point, an exponential increase in the evaporation heat flux can be seen from models adopting the logarithmic driving force (Opschoor's model and PVAP). The significant increase in the evaporation heat flux near the boiling point may overcome conduction heat flux from the beginning of the cryogenic pool vaporization (as the pool is initially considered near boiling point). It may lead to the evaporative cooling (decrease in temperature) of the liquid pool.

The substantially high prediction of evaporation heat flux by Mackay and Matsugu's model, over the given pool temperature range, is the reason of the high *C* value adopted in the mass transfer coefficient of the model. The heat flux predicted by Mackay and Matsugu's model may keep the liquid cryogenic pool in evaporation regime over complete vaporization process.

For a wind speed of 10 m s^{-1} measure at 10 m high, the convective heat flux dominates the predicted evaporation heat flux by all the models, except Mackay and Matsugu's model, below 93 K pool temperature. As the pool temperature increases, the predicted convective heat flux decreases due to the decrease in the temperature gradient between the liquid pool and air. The convective heat flux gets lower than the evaporation heat flux (all models) at about 103 K and it keeps on decreasing with further increase in the pool temperature.

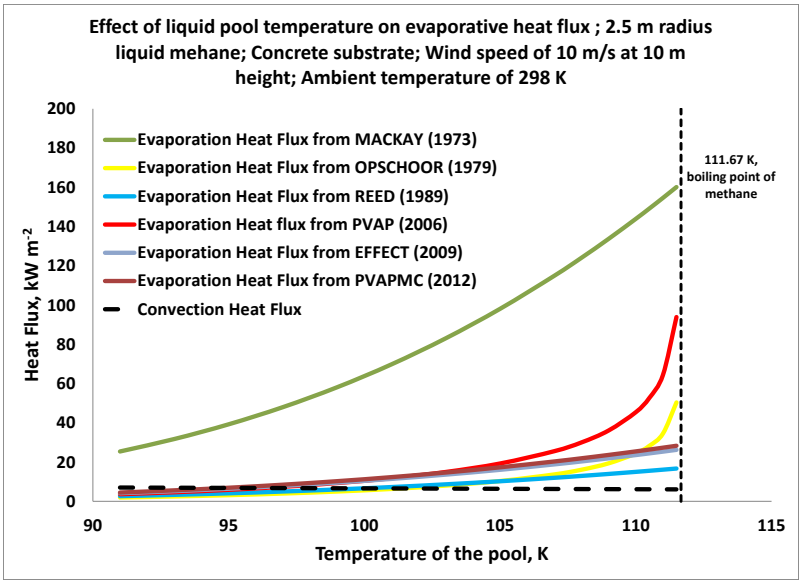

Figure 17: Predicted convective and evaporative heat flux versus liquid temperature for a liquid methane pool

To study the effect of wind speed on the predicted evaporative flux simulations were run for several fixed liquid methane pool temperature: 90K, 101K and 111 K (just below the boiling point of methane 111.67 K). The wind speed at 10 m height was varied from 1 to 15 m s^{-1}. The prediction of the convective heat flux is also calculated to compare with evaporative heat fluxes. The results are shown in Figure 18 to Figure 20.

For all the studied cases the predicted evaporative heat flux from the Mackay and Matsugu's model are significantly higher than the predicted evaporative heat flux from the other models. For liquid pool temperature of 91K, the predicted value of convective heat flux is higher than the evaporative heat flux for wind speeds higher than 4 m s^{-1} (Figure 18). As the liquid pool temperature increases, the relative importance of the convective heat flux decreases compared to the evaporative heat flux (Figure 19). When

the pool is close to the boiling point (111 K) the evaporative heat flux is always higher than the convective heat flux in the rage of wind speed investigated.

PVAP predicts a significantly higher value of the evaporative heat flux than the other evaporation models (except the one from Mackay and Matsugu) when the pool temperature is close to the boiling point. This may be explained by the fact that model adopting logarithmic driving force tends to provide high values of the evaporative heat flux close to the boiling point and for the same reason, evaporation heat flux predicted by Opschoor's model (adopting logarithmic driving force) increases as well.

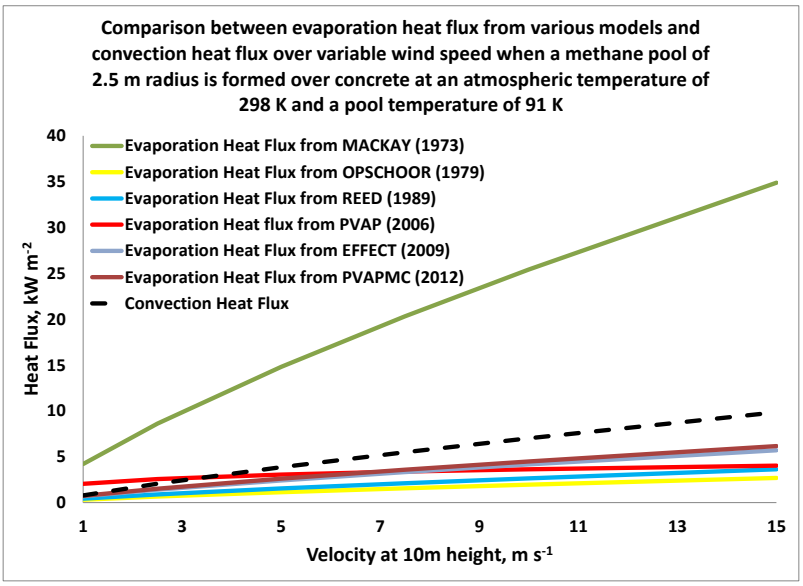

Figure 18: Effect of wind speed on convection and evaporation heat flux for a liquid methane pool at 91 K

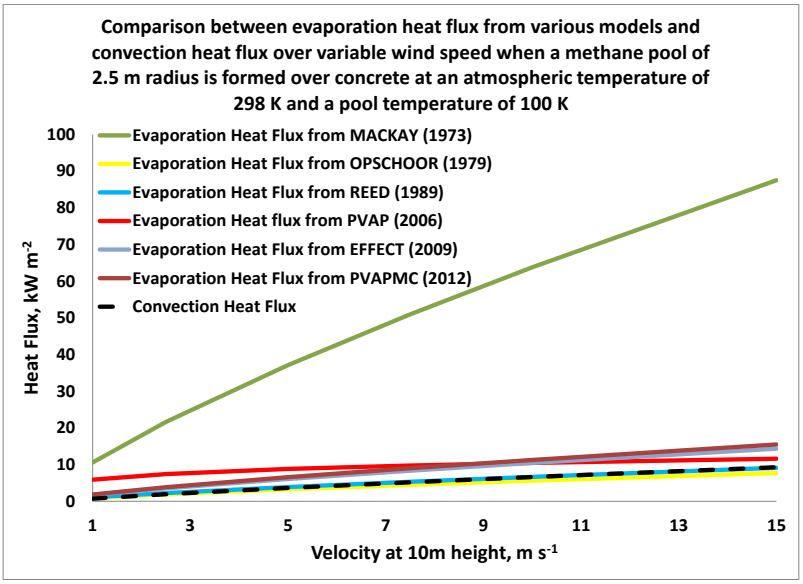

Figure 19: Effect of wind speed on convection and evaporation heat flux for a liquid methane pool at 100 K

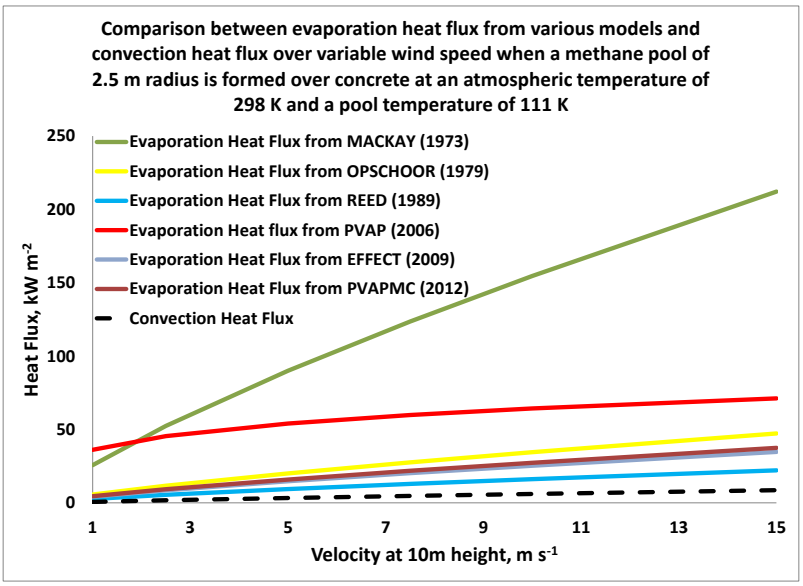

Figure 20: Effect of wind speed on convection and evaporation heat flux for a liquid methane pool at 111 K

The evaporative heat flux will have a direct effect on the duration of the boiling regime (time to switch from boiling to evaporation regime), the liquid pool temperature and therefore the resulting convective heat flux. It is necessary to perform the dynamic simulation of the pool vaporization.

6.3 Dynamic of the Vaporization – Change of Vaporization Regime

Dynamic liquid pool vaporization simulations were performed with the conditions set in the base case using the following models: REED 1989, PVAP 2006 and EFFECTS 2009. The heat fluxes from conduction, convection and evaporation were plotted against time as well as the resulting liquid pool temperature. The liquid temperature curve is used to observe the change of vaporization regime.

6.3.1 Simulations Using REED 1989 Model

Figure 21 presents the conduction, convection and evaporation heat fluxes predicted with the simulation tool using REED 1989 model for evaporation. It can be seen that the earlier part of pool vaporization (up to 100 s) is dominated by conduction. The relatively high conductive heat flux leads to an extremely fast warming of the liquid pool (few seconds) to the liquid boiling point. The pool enters the boiling regime and the temperature of the liquid pool stays constant. The conductive heat flux decreases relatively rapidly with time as the substrate cools down (due to boiling and evaporation) and becomes lower than convection heat flux at approximately 750 s.

The predicted evaporative heat flux is higher than the other two heat fluxes after t=100 s and for the rest of the entire duration of the pool vaporization. At t=252 s the evaporative heat flux overcomes the combined conductive and convective heat fluxes and the pool enters the evaporation regime characterized by the evaporative cooling of the pool. This evaporative cooling will also increase the temperature difference between the liquid and the surrounding such enhancing the convective heat transfer.

6.3.2 Simulations Using PVAP 2006 Model

PVAP uses the logarithmic driving force in the evaporation equation (high predicted evaporative heat flux near boiling point as shown in Figure 17). The liquid methane being spilled close to the boiling point, evaporation heat flux is initially very high as shown in Figure 22. This value is higher than the one predicted by Reed's evaporation model. Within the 10 second following the start of the simulation, evaporative heat flux dominates the conduction heat flux and the pool shifts to the evaporation regime until all the liquid pool is vaporized. Figure 22 shows that the pool vaporizes essentially under the evaporation regime, which is an unexpected result.

Opschoor's model will also show a very similar behavior (as both models adopt logarithmic driving force) and therefore, will not be discussed here.

6.3.3 Simulations Using EFFECTS 2009 Model

The trends using EFFECTS model are very similar to the ones obtained from Reed's model, as shown in Figure 23. However, the predicted duration of the boiling

regime is smaller than predicted by Reed's model. PVAP-MC provides similar results as EFFECTS (both models adopt linear driving force).

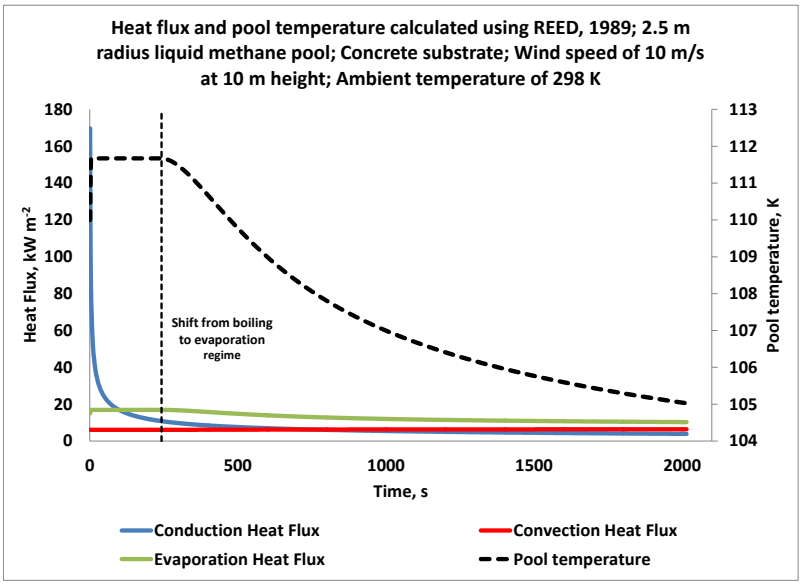

Figure 21: Conductive, convective and evaporative heat fluxes and liquid pool temperature using REED 1989 model during a methane spill over concrete

It is important to note that the above models, in the conditions of the simulations, regardless of their nature (logarithmic or linear expression of the driving force for evaporation) will predict that the dominant vaporization mechanisms for the entire duration of the simulation is evaporation (sometime with no or very short boiling period) which was unexpected.

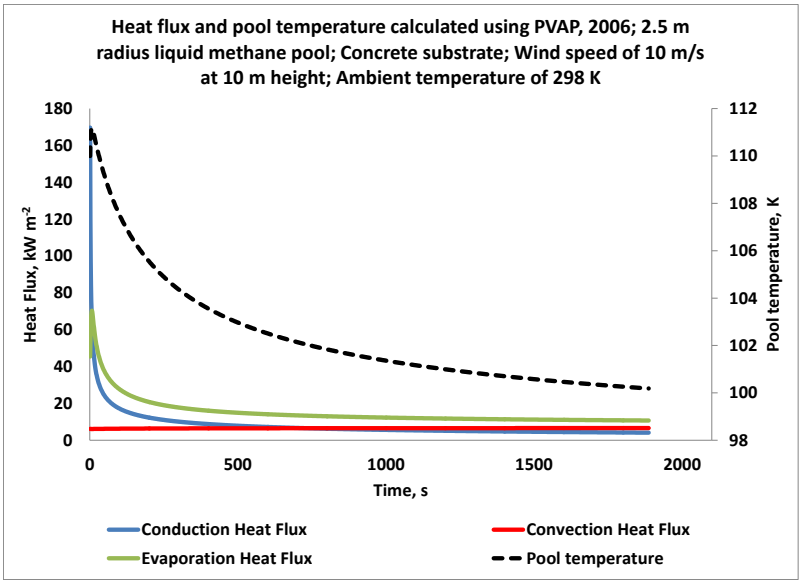

Figure 22: Conductive, convective and evaporative heat fluxes and liquid pool temperature using PVAP 2006 model during methane spill over concrete

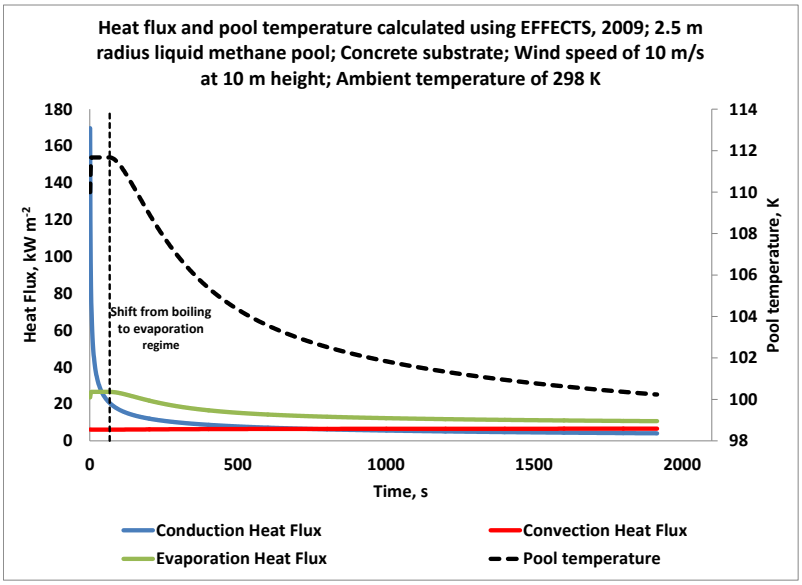

Figure 23: Conductive, convective and evaporative heat fluxes and liquid pool temperature using EFFECTS 2009 model during methane spill over concrete

6.4 Effect of Substrate Type on the Vaporization Regime

Several simulations were run to understand the effect of substrates of different thermal conductivity (concrete and polystyrene) on the vaporization results. The polystyrene is a material of lower conductivity than concrete. The following evaporation models were used: Mackay & Matsugu 1973, Reed 1989, PVAP 2006 and PVAP-MC 2012. The conditions of the simulations are similar to the base case using different substrate with their corresponding thermal properties

With Mackay & Matsugu's model (Figure 24), for both substrates, the pool temperature decreases from the beginning of the simulations, indicating that the vaporization mechanism is only evaporation. The liquid temperature decreases faster with polystyrene than concrete. The liquid cooling effect induced by evaporation is more important with polystyrene as the conductive heat transfer is less effective on this material.

A similar behavior is observed with PVAP, 2006 (Figure 25). The liquid cooling effect is however less important for both substrate than with the Mackay & Matsugu's model, as the later model predict lower evaporative heat flux (Figure 20). With Reed's model (Figure 26), for the polystyrene substrate, the drop in temperature of the pool can be seen as soon as the vaporization starts which means that the pool is in the evaporation regime right from the beginning. For the concrete substrate, the model predicts that pool will boil for approximately 5 minutes before the temperature drops down. With Reed's model it is predicted that the change of the substrate results in the change in the vaporization mechanism.

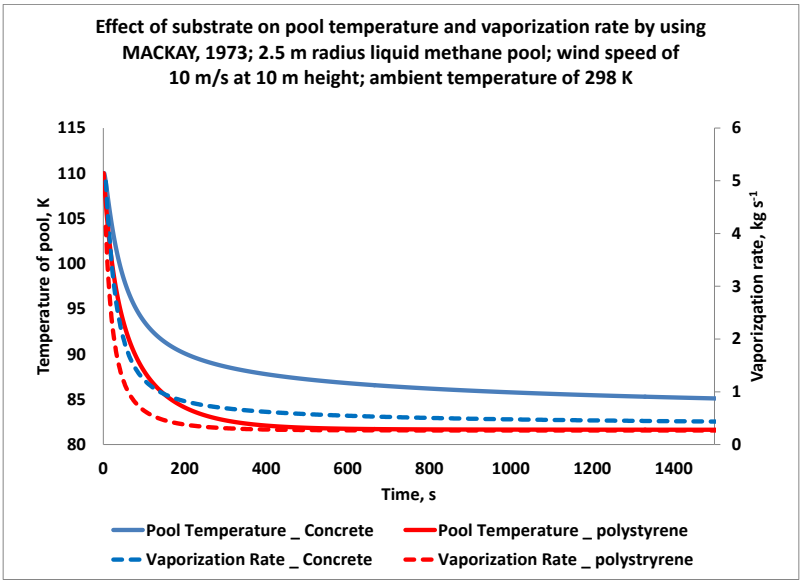

Figure 24: Effect of substrate on pool temperature using Mackay & Matsugu 1973

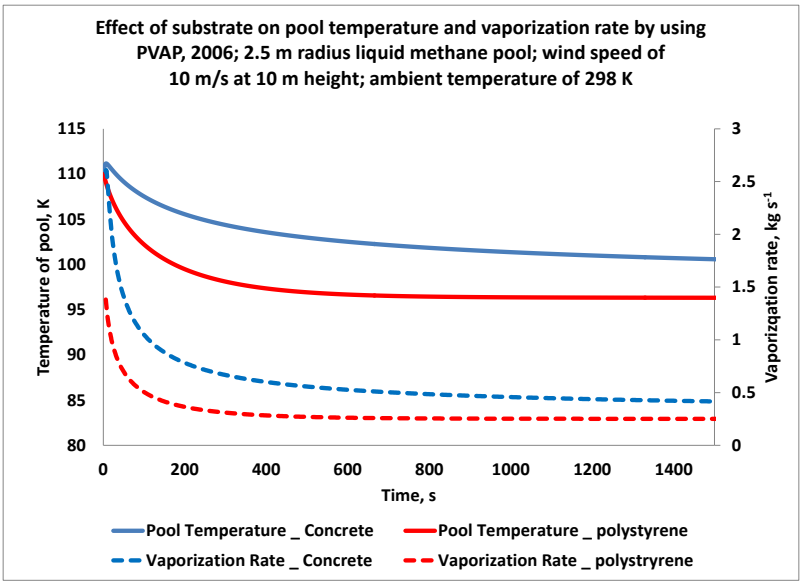

Figure 25: Effect of substrate on pool temperature using PVAP 2006

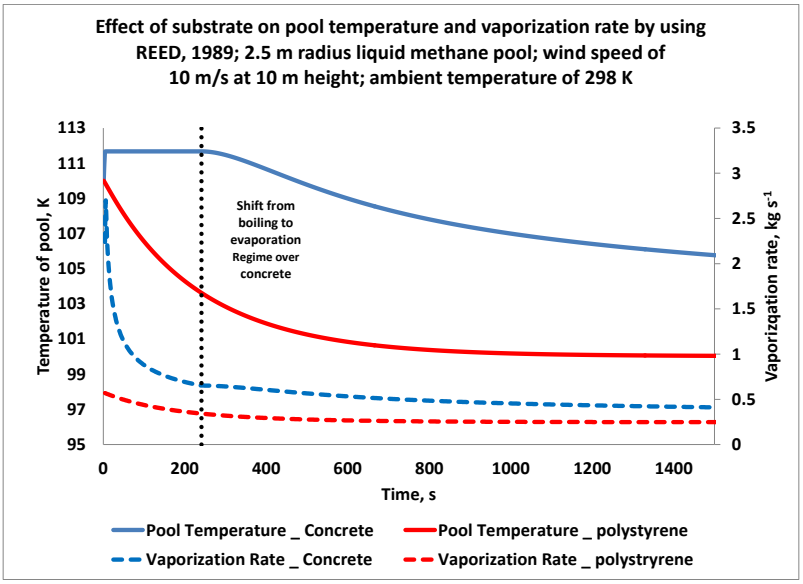

Figure 26: Effect of substrate on pool temperature using Reed 1989

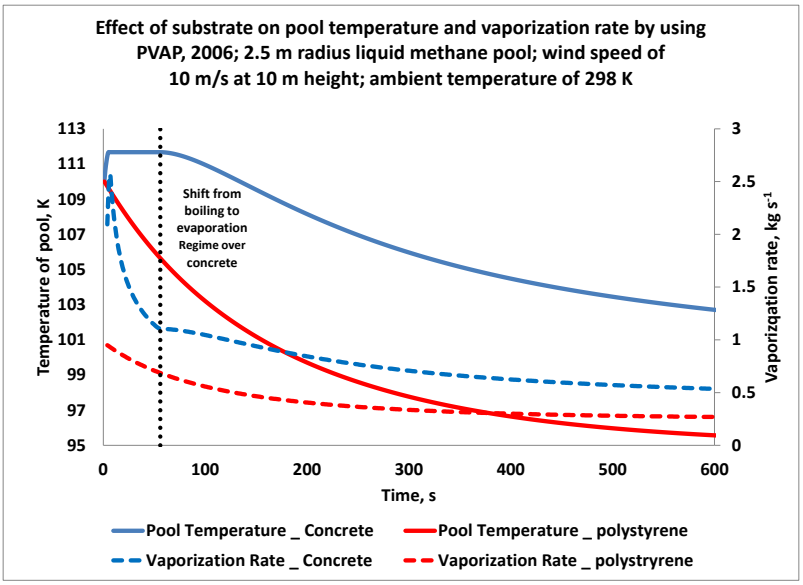

Figure 27: Effect of substrate on pool temperature using PVAP-MC 2012

As predicted with the model, an insulated substrate may lead to the complete absence of boiling phase. Similar behavior was observed with the PVAP-MC 2012

(Figure 27). Here again the polystyrene substrate prevents the pool from staying in the boiling regime. According to these results, boiling seems to be unlikely on insulated substrates. Again this is an unexpected result that requires experimental validation.

6.5 Effect of Pool Radius on the Vaporization Rate

The effect of the radius of the pool on the vaporization was investigated. The simulations were run with the condition set in the base case but with liquid pool radius of 0.5 m, 1 m, 2 m, 2.5 m, 5 m, 10 m, 50 m and 100 m. The evaporation model used for the simulation is Reed, 1989. Figure 26 shows that the vaporization of the pool is performed in both boiling and evaporation regime. The duration of boiling is relatively short compared to evaporation. Figure 27 shows that duration of the boiling regime tends to increase with the pool radius. The pool boiling duration seems very sensitive to the pool radius for relatively small pools (radius < 10 m).

The analysis seems to indicate that relatively small scale vaporization experiments would be more likely to show evaporation and evaporative cooling than larger scale ones. It is to be noted that with this model, even with relatively large pools (100 m radius) the duration of the boiling seems relatively short (< 500 second) before evaporative cooling is observed. This needs to be experimentally verified.

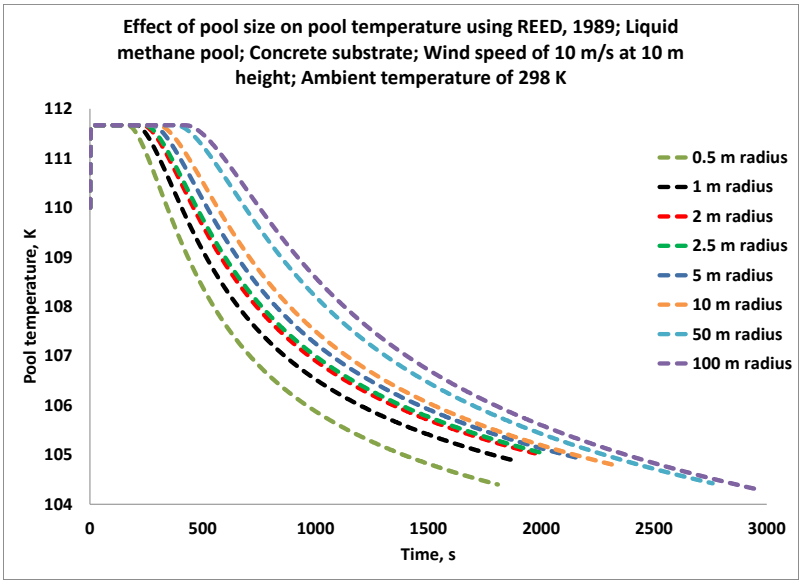

Figure 28: Effect of pool size on temperature of the pool, using Reed 1989

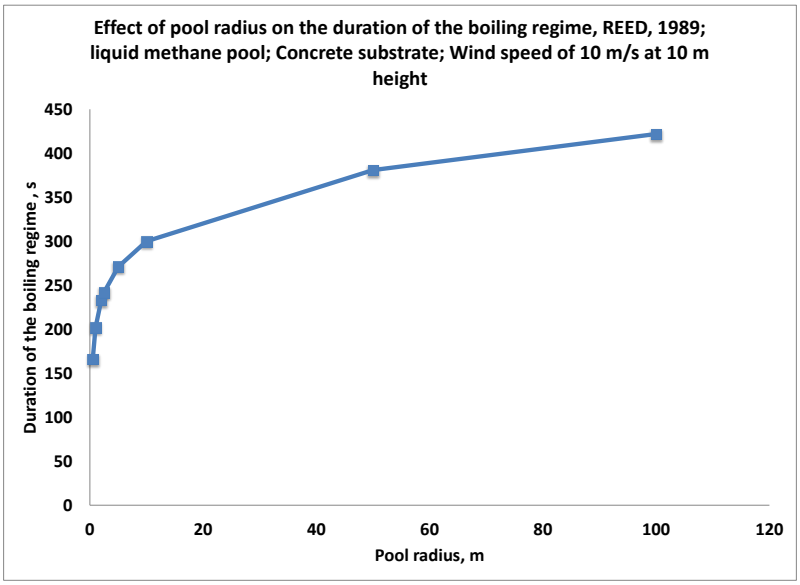

Figure 29: Effect of pool size on the duration of the boiling regime, using Reed 1989

6.6 Effect of Ambient Temperatures on the Vaporization Rate

The effect of the ambient temperature on the vaporization was investigated. The simulations were based on the base case three different ambient temperatures: 273 K, 298 K, and 323 K. The evaporation model used for the simulation is Reed, 1989.

As expected, the higher the ambient temperature the higher the vaporization rate (Figure 30). Consequently the time to completely vaporize the pool decreases as the ambient temperature decreases (Figure 31). This can be directly related to the fact that the ambient temperature affects the convective heat flux. The ambient temperature also has an effect on the predicted duration of the boiling regime. As shown in Figure 30 and Figure 32, the higher the ambient temperature (the higher the convective heat flux), the longer the duration of the boiling regime.

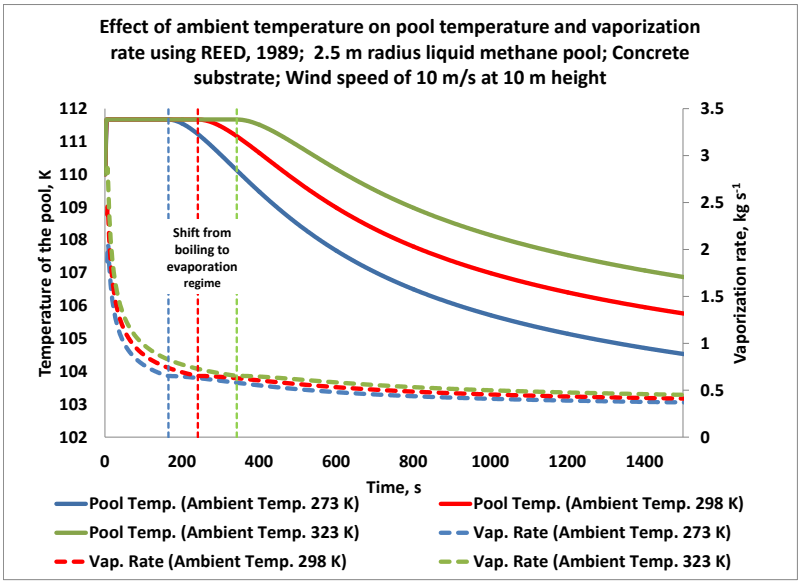

Figure 30: Effect of the ambient temperature on the pool temperature and the vaporization rate, using Reed 1989

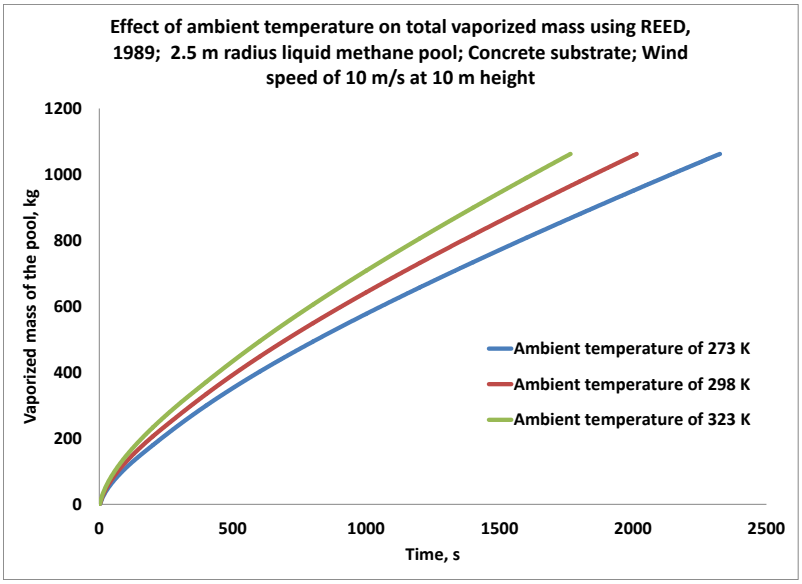

Figure 31: Effect of the ambient temperature on vaporized mass, using Reed 1989

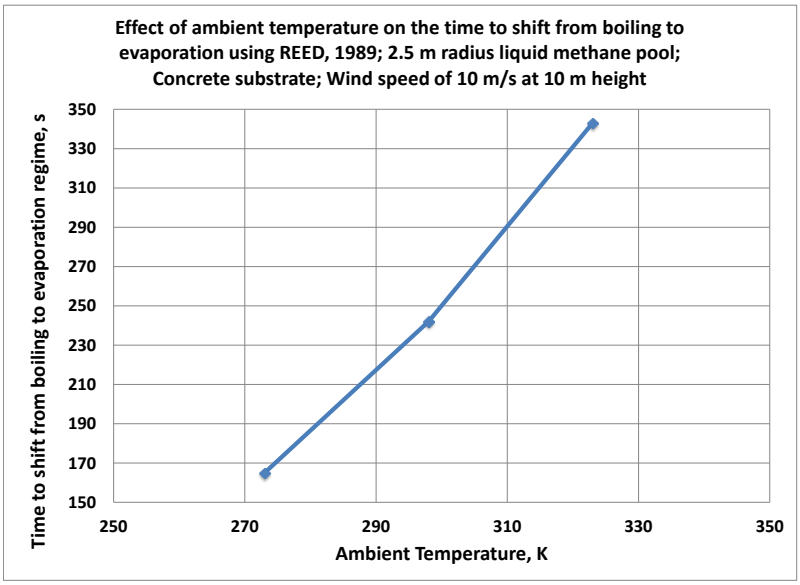

Figure 32: Effect of the ambient temperature on the duration of the boiling regime, using Reed 1989

6.7 Dynamic Pool Vaporization - Comparison of the Evaporation Models

Dynamic liquid pool vaporization simulations for the defined base case were performed to compare the predictions of the following evaporation models in terms of vaporization rate, pool temperature, and dominant vaporization regime (boiling and/or evaporation): Mackay and Matsugu 1973, Opschoor 1979, Reed 1989, PVAP 2006, EFFECTS 2009 and PVAP-MC 2012.

Regardless of the evaporation model used, the predicted value of conduction heat flux is very high (about 170 $kW.m^{-2}$) at the start of cryogenic pool vaporization. As the vaporization progresses, the substrate cools down and conduction heat flux decreases. Although the pool temperature changes over time but, unlike convection and evaporation heat flux, conduction heat flux does not seem to be highly sensitive to the pool temperature and gives approximately the same result regardless of the evaporation model under consideration (Figure 33). The observed changes in the simulation results can therefore be essentially linked to the convective and evaporative heat fluxes.

The driving force for the convective heat flux is the temperature gradient between the liquid pool and air. The excessive cooling of the pool predicted by Mackay and Matsugu's model leads to a high temperature gradient between the liquid pool and the air, therefore, high value of convection heat flux is observed when using this model (Figure 34). When Reed's evaporation model was used, the convective heat flux calculated is constant (6.1 $kW\ m^{-2}$) for about 300 second. This may be explained by the fact that, the liquid pool being in the boiling regime for the 300 second, the pool temperature does not change and therefore the convective heat flux is constant.

The predicted evaporation heat flux is particularly different for different evaporation models as shown in Figure 35. The difference is significant at early stage of pool vaporization (initial 500 second). Comparatively high values of evaporation heat flux can be seen for the models adopting logarithmic driving force, except Mackay and Matsugu's model. It has already been discussed in section 6.2 that evaporation heat flux is directly affected by the pool temperature. The simulation considered a liquid methane pool initially at a temperature close to the boiling point and therefore the evaporation heat flux is relatively high for the early stage of pool vaporization. It is also interesting to point out that the evaporative cooling caused by high evaporation heat flux will decrease the temperature of the pool and the evaporation heat flux, after reaching a maximum value at liquid boiling point, will tend to decrease.

The predicted pool temperature using different evaporation models is shown in Figure 36. It also shows the pool temperature when the simulation is performed without taking into account evaporation (boiling point of liquid methane). The evaporation models adopting linear driving force, except Mackay and Matsugu's model, predicts pool boiling of relatively short duration (about 75 second for PVAP-MC, 100 seconds for EFECTS, and 300 seconds for Reed's evaporation model) followed by evaporation whereas the pool temperature predicted by evaporation models adopting the logarithmic driving force (PVAP and Opschoor's model) does not even enter the boiling regime at any stage of the vaporization and keeps on decreasing with time. The decrease in the cryogenic liquid pool temperature predicted by all the models at different stages of pool vaporization is unexpected.

The vaporization rate without taking into account evaporation (only boiling throughout pool vaporization) is lower than the vaporization rate when evaporation heat flux is included (Figure 37). The evaporation models adopting the logarithmic driving force shows high vaporization rate since these models predict pool evaporation from the initial stage of vaporization whereas the evaporation models adopting linear driving force for evaporation show boiling for short duration. It can be seen from Figure 38 that as the models predict the regime shift (boiling to evaporation) the vaporization rate of the liquid pool increase. It may indicate the inadequacy of the evaporation models near boiling point of the cryogenic liquid.

Figure 39 shows that taking evaporation into account (by different models) decreases the time for the complete pool vaporization (minimum for Mackay and Matsugu's model and maximum for Reed's) compared to the pool vaporization time under complete boiling conditions.

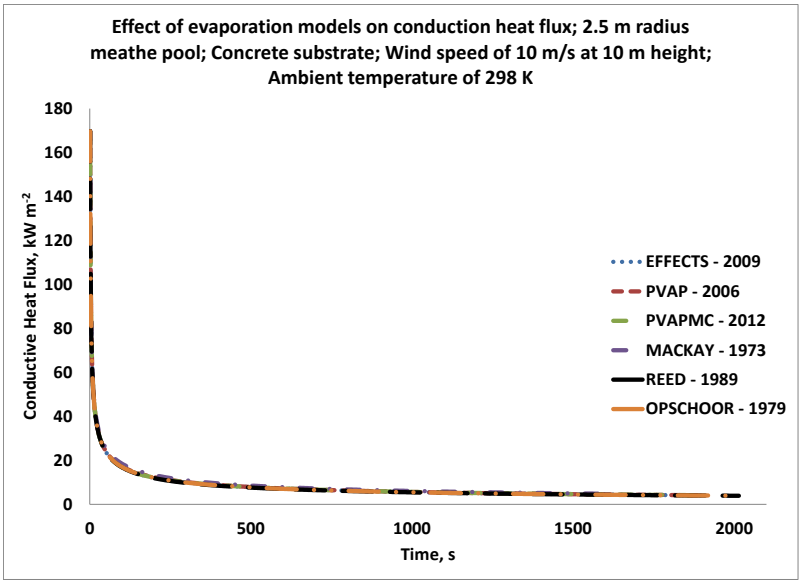

Figure 33: Conductive heat flux over time during methane spill over concrete

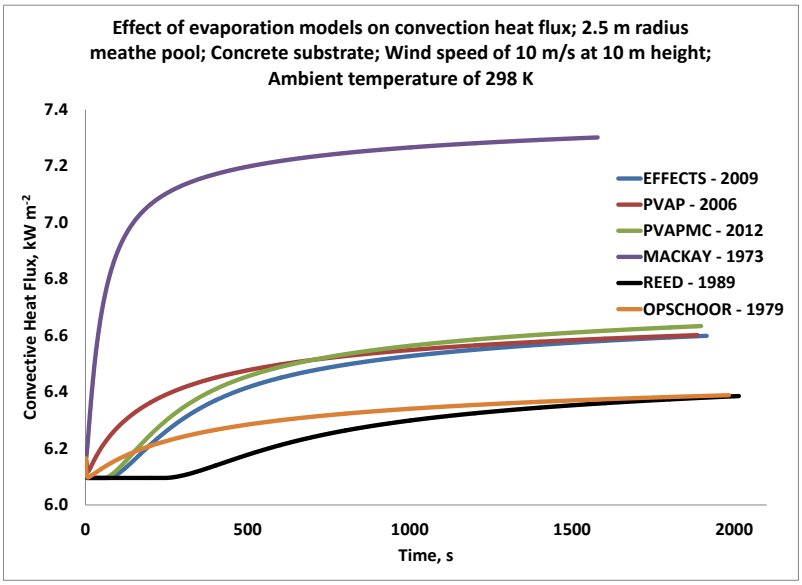

Figure 34: Convective heat flux over time during methane spill over concrete

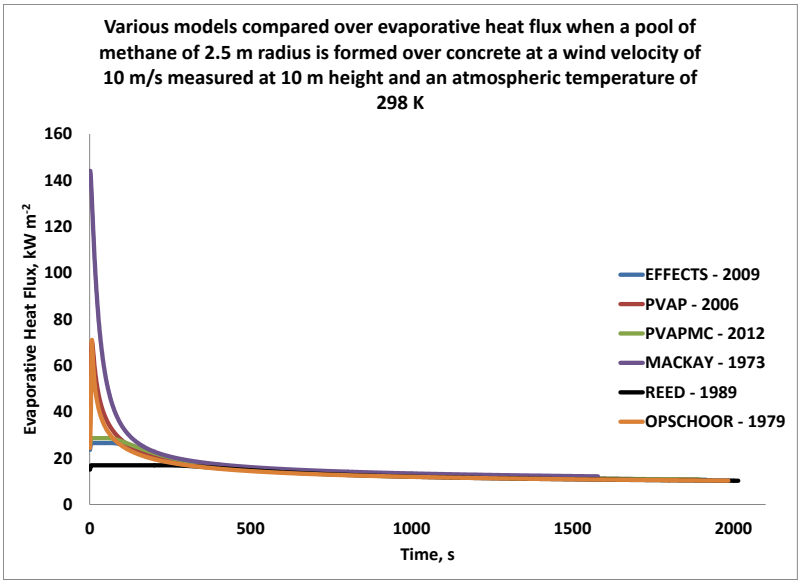

Figure 35: Evaporative heat flux over time during methane spill over concrete

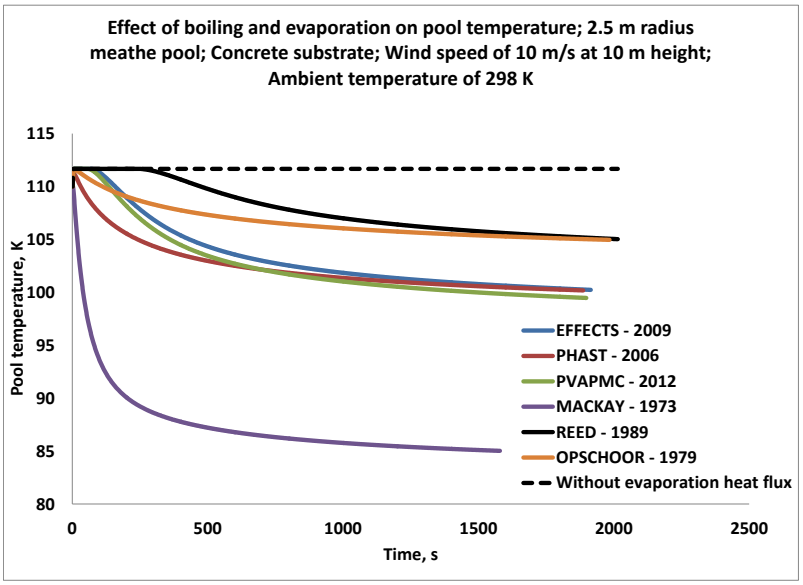

Figure 36: Temperature of the pool of methane as a function of time

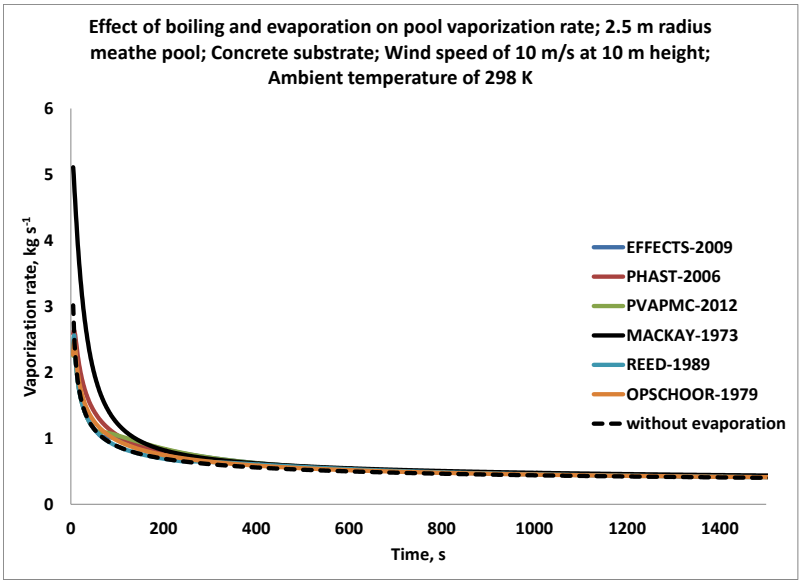

Figure 37: Vaporization rate of the methane pool as a function of time

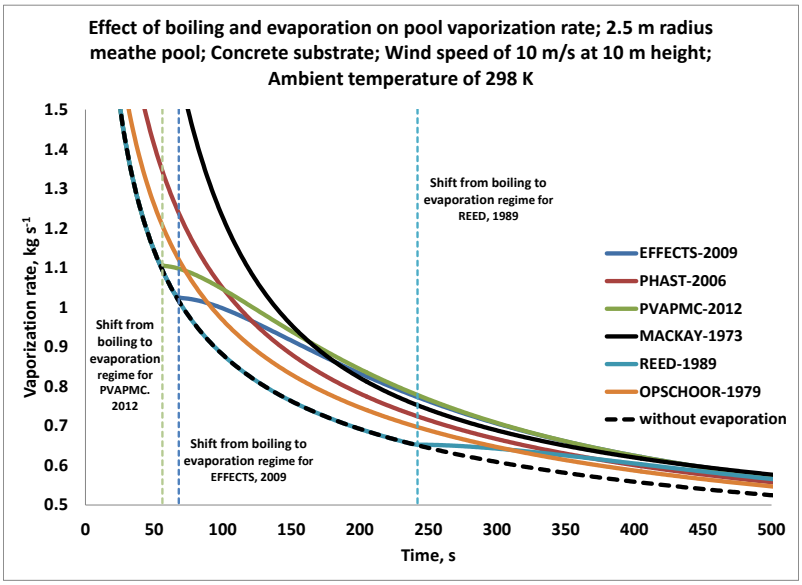

Figure 38: Change in the vaporization rate due to the shift from boiling to evaporation regime

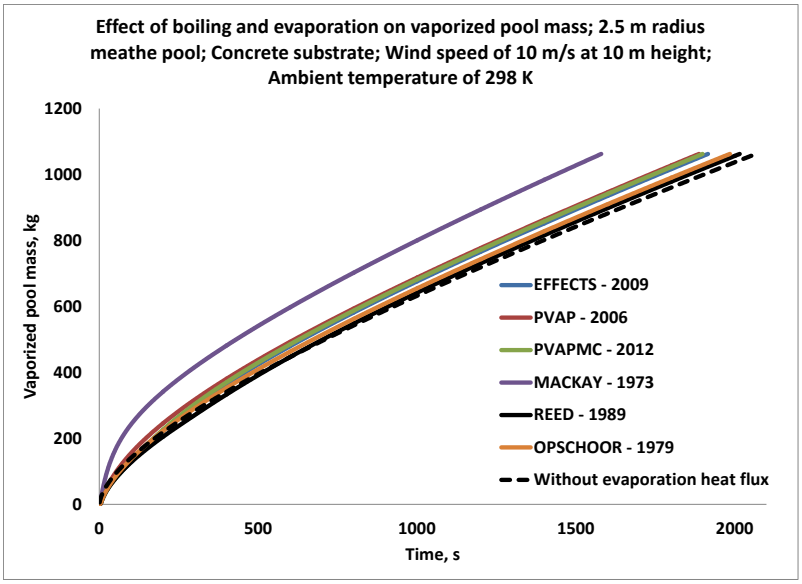

Figure 39: Total vaporized mass of methane as a function of time

7. VALIDATION OF THE VAPORIZATION MODELS

Following the previous verification work, the validation of the models against a set of experimental data generated with liquid nitrogen at Ras Laffan Industrial City (RLIC), Qatar in 2012. The experiment was a scale up of small scale experiments performed in the laboratory of Texas A&M University at Qatar [31].

This experiment was carried out using liquid nitrogen (LN_2) spilled on the polystyrene. The size of containment was 0.48 m x 0.48 m x 0.1 m. The wall and base thickness were 0.15 m. The box was entirely made of polystyrene which tends to limits the heat losses by conduction. The box was equipped with embedded heat flux plates and thermocouples in its base and walls, and the heat losses via the box walls were measured. A discharge pipe was used to feed LN_2 to the polystyrene box, however the discharge flow was not monitored and thus the initial data of filling could not be analyzed and the analyses may start only when the spill was stopped. The box itself was placed in a wind tunnel, 2.04 m wide 0.855 m tall and 12 m long, which was especially designed to isolate the box from natural wind and to ensure a controllable and stable airflow. A 1.2 m diameter variable speed electric fan was placed at the entry of the tunnel and the center of the polystyrene box was located 5.64 m from the outlet of the fan. The wind data were measured by two ultrasonic anemometers (81000, R.M. Young USA) at two different positions. 11 thermocouples were placed inside the containment of the box to obtain the temperature of the pool at different depths. The thermocouples locations from the bottom of the containment are summarized in Table 11. Also,

thermocouples and humidity sensors were placed to record the temperature and humidity inside the wind tunnel. The polystyrene box was placed on a balance to measure the remaining mass of the pool (mass measurement resolution was 10 g). The experimental setup is shown in Figure 40 and its conditions are tabulated in Table 12.

(a)

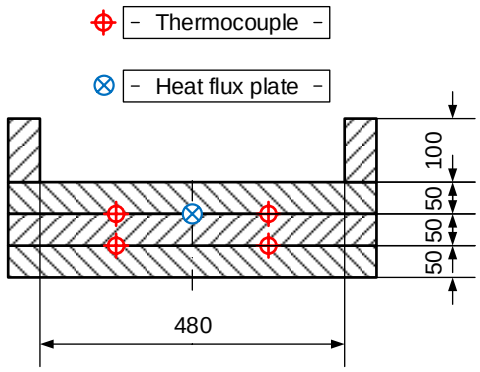

(b)

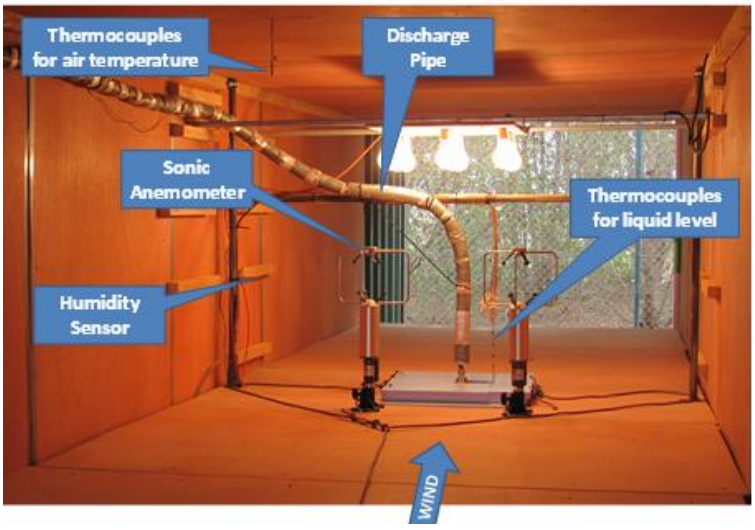

Figure 40: Dimensions of the polystyrene box (a) and the experimental setup (b)

All models were run for the same scenario with the MATLAB tool inputs shown in Table 12. A comparison has been made to observe the vaporization of the LN_2 pool

(Figure 41) and pool temperature (Figure 42) measured during the experiment and predicted by the models.

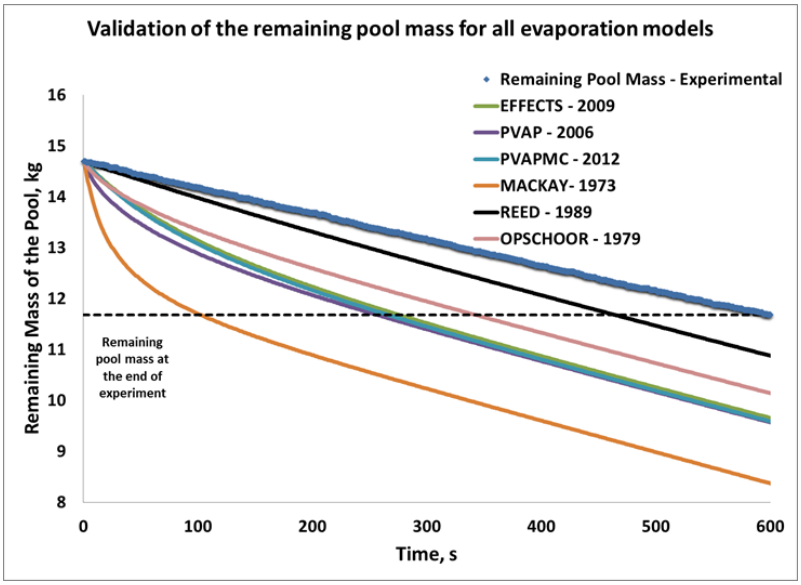

Figure 41: Validation of evaporation models for the mass of the pool

The predictions of Reed's model are nearest to the experimental values whereas results of Mackay and Matsugu's model show maximum deviation from the experimental observation. However, it can be seen that none of the models demonstrate similar behavior to the experimentally measured pool temperature (Figure 42), which constantly stays at the boiling point. For example, Reed's model predicts pool cooling after 100 s, and this is simply not observed experimentally.

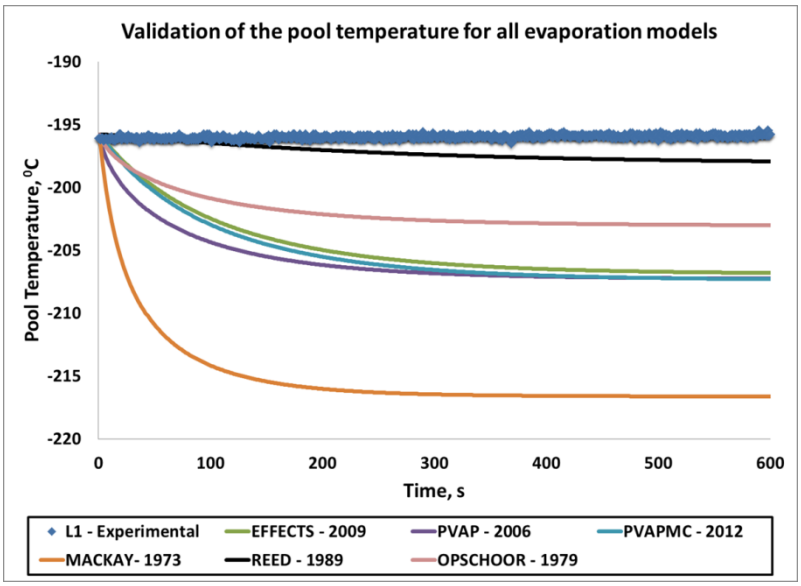

Figure 42: Validation of evaporation models for the temperature of the pool

The pool mass calculated from the MATLAB program for the boiling pools (ignoring evaporation) is consistent with the experimentally measured pool mass as shown in Figure 44. There is still slight deviation between the prediction and the measurement but it is not as extensive as it was observed for evaporation models. The nonconformity of this model can be perhaps addressed by looking deeply into conduction and convection models. An improvement in those models can potentially give better agreement with experimental data, which should be investigated in the future.

Table 11: Position of the thermocouple (level) inside the liquid pool

Thermocouple	Height from Bottom, mm
L – 01	1
L – 02	11
L – 03	21
L – 04	31
L – 05	40
L – 06	51
L – 07	62
L – 08	71.5
L – 09	81
L – 10	91
L – 11	101.5

Table 12: Simulation inputs for the validation

Parameters	Inputs
Substance	LN_2
Substrate	Polystyrene
Initial Pool Mass, kg	14.69
Pool Radius, cm	0.24
Temp. of Atmosphere, K	309
Spill Temp., K	77.35
Temp. of Substrate, K	309
Wind Speed at 30.5 cm height, m s^{-1}	2.99

A model for boiling pool (ignoring evaporation) may be sufficient to predict the temperature of the pool for such a scenario (Figure 43), such putting into question the need to adopt evaporation into the source term calculation at least for such small scale (48 cm diameter pool) This also brings into question the possibility of evaporative cooling for the spill of cryogenic liquid, as such observation was not done here. As shown in Figure 28 the size of the pool tends to increase the duration of the boiling regime. So experiments at larger scale are necessary to conclude on the possibility of evaporative cooling and provide an improvement of the evaporation models for cryogenic pools.

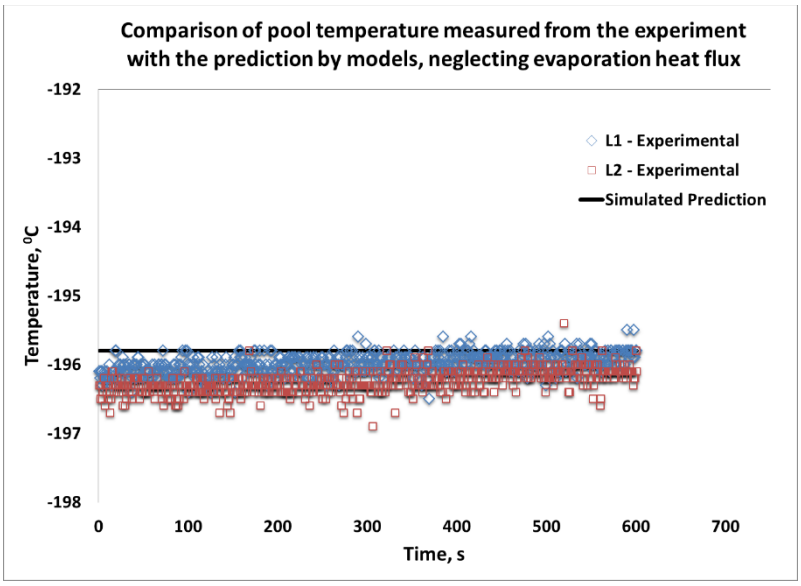

Figure 43: Comparison of pool temperature from experimental measurement and model prediction, negleting evaporation heat flux

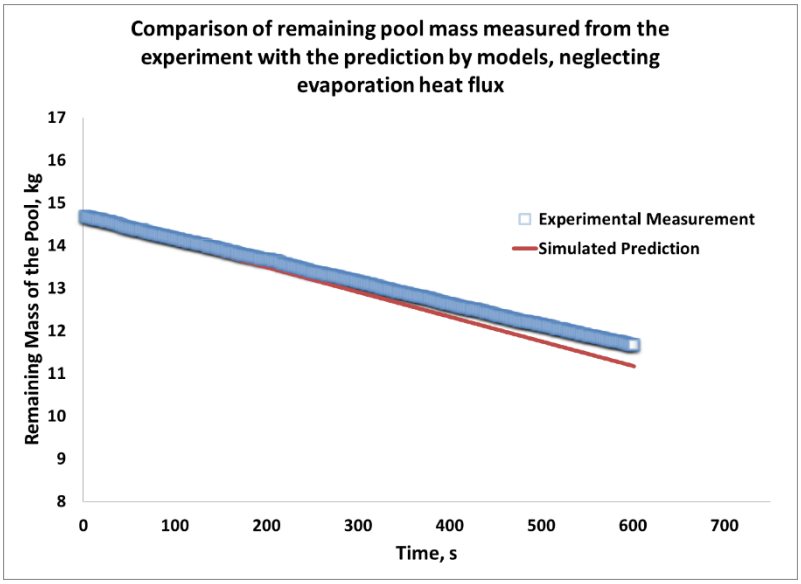

Figure 44: Comparison of remaining mass of the pool from experimental measurement and boiling model prediction

8. CONCLUSION AND RECOMMENDATIONS

A comprehensive review of state of the art evaporation models for liquid spills was performed. Evaporation models are divided into two categories on the basis of the expression of the driving force, namely logarithmic and linear expression. This review showed that there is still a substantial room for improvement of these models since they have been developed for non-cryogenic liquids, although the range of application of those models was not explicitly limited to non-cryogens. The validation of the models for cryogenic liquids was not performed by any author and hence their application remains questionable.

A simulation program was built under MATLAB to simulate the spill of a cryogenic liquid over a solid substrate under given weather conditions. The model takes into account conduction, convection and evaporation heat transfer mechanisms and performs the integration of an energy and mass balance on a vaporizing pool. The model was verified against PHAST 6.7.

A set of simulation with liquid methane on solid substrate was done to understand the contribution of the different heat transfer mechanisms on the vaporization regime and the pool temperature. A sensitivity analysis to the following parameters was done: pool radius, substrate type, wind speed, and surroundings temperature.

The simulations using the MATLAB tool and their comparison with experimental data provided the following key findings:

- Near the boiling point relatively high values of evaporation heat flux are predicted by all the models investigated, the models adopting logarithmic driving force showing significantly higher evaporative heat fluxes than the ones adopting linear driving force. At cryogenic liquid boiling point the evaporation heat flux calculated from logarithmic evaporation models tend to infinity. Numerical restrictions in the program may help to avoid the calculation error. This result is not surprising as logarithmic evaporation models have been developed essentially for non-boiling pools. As a consequence, the simulation with the logarithmic evaporation models simply predicts that *the vaporization phenomena for the cryogenic liquid pool will always be evaporation, with no boiling.* The models adopting linear evaporation driving force predicts cryogenic pool boiling *but the duration of boiling regime is relatively short (the vaporization being mainly by evaporation)*. These results were unexpected and need to be experimentally validated against large scale experiments.
- Both convection and evaporation heat flux are function of wind speed and increases with the increase in the wind speed. The convection heat flux near the boiling point may be lower than the evaporation heat flux for a range of wind speed (1 m $s^{-1}$to 15 m s^{-1}) but far from the boiling point convection heat flux is generally observed to be higher than the evaporation heat flux except for low

wind speed. This suggests an overall *dominance of evaporation heat flux over convection heat flux at low wind speed at any given pool temperature*.

- For the substrates with low thermal conductivity (i.e. polystyrene), all the evaporation models under consideration predict a drop in cryogenic liquid pool temperature from the start of the vaporization process. T*he models adopting logarithmic evaporation driving force* showed drop in temperature over entire vaporization period which indicates *the complete absence of the boiling phase when regardless of the substrate.* However, *linear evaporation models show pool boiling for thermally conductive substrates, but for a relatively small time followed by liquid pool evaporation.* As the vaporization regime shifts, the vaporization rate also changes.
- The duration of the boiling regime predicted by the linear evaporation models seems to be sensitive to the size of the pool: the greater the pool size, the longer the pool boiling time.
- Effect of ambient temperature on the vaporization rate of the pool is up to expectation: it was observed that an increase in the surroundings temperature leads to an increase of the vaporization rate, essentially due to the fact that it enhances the heat supplied to the pool by convection. This also tends to increase the duration of the boiling regime.
- The vaporization rate calculated with a boiling pool model (ignoring evaporation completely) provides lower vaporization rates than models taking into account

evaporation. It is highly unexpected for the vaporization rate to be more in evaporation regime than in boiling regime.

- The comparison of the evaporation models against experimental data (experiment done with liquid nitrogen at a relatively small scale) showed that none of them seems to describe the vaporization of a cryogenic pool. It may be that the evaporation models are inadequate for use at temperature close to the boiling point. It was observed that the use of a model assuming only boiling as vaporization mechanism (neglecting evaporation completely) is sufficient to describe predicts the vaporization of the liquid at this scale. Similar analysis needs to be done against experimental data obtained at large scale to conclude on the possibility of evaporation and evaporative cooling.

The results of the simulation work showed that there is a need is to design experiments for large scale to comprehensively assess the evaporation phenomenon. To date, evaporation is taken into account into widely used consequence modeling software (e.g. PHAST) which predicts very sort boiling duration and a vaporization dominated by evaporation. Also, the experiments should not only be performed using LN_2 but should cover a wider range of cryogenic liquids (LNG, air, ammonia, etc.). The use of liquid ammonia in the experiments could possibly address the claim of TNO [13] that the temperature of liquid ammonia pool can drop from its boiling point (-33°C) to -75°C, which has not been confirmed by any experiment.

If evaporation is observed from those experiments, ultimately a model providing a better description of evaporation for cryogenic pool must be developed.

BIBLIOGRAPHY

1. BP Review. *British Petroleum - Statistical Review of World Energy*. London; 2013:45. Available at: http://www.bp.com/content/dam/bp/pdf/statistical-review/statistical_review_of_world_energy_2013.pdf.

2. Olewski T, Véchot L, Mannan MS. Study of the vaporization rate of liquid nitrogen by small and medium scale experiments. Rademaeker E De, Fabiano B, Buratti SS, eds. *Chem Eng Trans*. 2013;31(1):133–138. Available at: http://www.aidic.it/cet/.

3. Carslaw HS, Jaeger JC. *Conduction of Heat in Solids*. 2nd ed. Oxford University Press, USA; 1986:520.

4. Véchot L, Olewski T, Osorio C, Basha O, Liu Y, Mannan S. Laboratory scale analysis of the influence of different heat transfer mechanisms on liquid nitrogen vaporization rate. *J Loss Prev Process Ind*. 2013;26(3):398–409. doi:10.1016/j.jlp.2012.07.019.

5. PHAST 6.54. PVAP - Technical Reference Documentation. 2006:39.

6. Fleischer FT. *SPILLS: an evaporative/air dispersion model for chemical spills on land*. Shell Development Company, Westhollow Research Center; 1980.

7. The Swiss Wind Power Data Website. Wind Profile Calculator. *METEOTEST*. Available at: http://www.wind-data.ch/tools/profile.php?lng=en. Accessed July 20, 2013.

8. Lee K-W. A methodology for assessing risk from released hydrocarbon in an enclosed area. *J Loss Prev Process Ind*. 2002;15(1):11–17. doi:10.1016/S0950-4230(01)00017-1.

9. Webber DM, Witlox HWM. PVAP - Verification. 2005:42.

10. Mackay D, Matsugu R. Evaporation rates of liquid hydrocarbon spills on land and water. *Can J Chem Eng*. 1973;51(4):434–9.

11. Opschoor G. Methods for the calculation of the physical effects of the escape of dangerous material (liquids and gases). *TNO Yellow B*. 1979:Chapter 5.

12. Reed M. The physical fates component of the natural resource damage assessment model system. *Oil Chem Pollut*. 1989;5:99–123.

13. Trijssenaar-Buhre IJM, Sterkenburg RP, Wijnant-Timmerman SI. An advanced model for spreading and evaporation of acidentally released hazardous liquids on land. *Safety, Reliab Risk Anal Thepry, Methods Appl Martorell al*. 2009:2363–2400.

14. Mahgerefteh H, Fernandez MI, Harper M, Witlox HWM. An integral model for pool spreading, vaporization and dissolution of hydrocarbon mixtures. In: *Hazards XXIII*. Liverpool, UK; 2012:466–472.

15. Himus G. The evaporation of water in open pans. In: *Vapor Absorption and Adsorption Sponsored by Inst. of Chern. Eng.* London; 1929.

16. Hine TB. Rate of evaporation of liquids in a current of air. *Phys Rev*. 1924;24.

17. D.Fitzgerald. Evaporation. *Trans. Am. Soc. Civil Eng*. 1886; 98(12):2073–2085.

18. Bird RB, Stewart WE, Lightfoot EN. *Transport Phenomena*. 2nd ed. John Wiley & Sons, Inc.; 2002. Available at: http://www.slideshare.net/abhishekg431/birdstewartlightfoottransportphenomena2nded2002.

19. Bird RB, Stewart WE, Lightfoot EN. *Transport Phenomena*. 1st ed. John Wiley & Sons, Inc.; 1960.

20. Directorate-General of Labor. *Experiment met acrylnitril*. Amsterdam; 1971.

21. Kawamura P, Mackay D. The evaporation of volatile liquids. *J Hazard Mater*. 1987;15:343–364.

22. Sherwood TK, Pigford RL, Wilke CR. *Mass Transfer*. McGraw-Hill; 1975:677.

23. Brighton PWM. Evaporation from a plane liquid surface into a turbulent boundary layer. *J Fluid Mech*. 1985;159:323–345. doi:10.1017/S0022112085003238.

24. Webber DM. Evaporation and boiling of liquid pools - a unified treatment. *Math Major Risk Assesment*. 1989:131–44.

25. DIPPR 801. Design Institute for Physical Properties Research (DIPPR 801). *Spons by AIChE (2005; 2008; 2009; 2010; 2011; 2012) DIPPR Proj 801 - Full*. 2012.

26. Webber DM. *Model for pool spreading and vaporization and its implementation in computer code GASP*. UKAEA Report, 1990; SRD R507.

27. PHAST 6.0. PVAP - Technical Reference Documentation. 2005.

28. Cavanaugh TA, Siegell JH, Steinberg KW. Simulation of vapor emissions from liquid spills. *J Hazard Mater*. 1994;38(1):41–63. doi:10.1016/0304-3894(93)E0111-E.

29. HGSYSTEM 3.0. *HGSYSTEM 3.0 Technical Reference Manual*. Chester; 1994.

30. James DW. The thermal diffusivity of ice and water between -40 and +60 deg. C. *J Mater Sci*. 1968;3:540–543.

31. Osorio C, Vechot L, Olewski T, Liu Y, Mannan S. Laboratory scale analysis of the influence of different heat transfer mechanisms on liquid nitrogen vaporization rate. In: *14th Annual Symposium Mary Kay OConnor Process Safety Center Beyond Regulatory Compliance Making Safety Second Nature*. Texas A&M University; 2011:494–511.

APPENDIX A

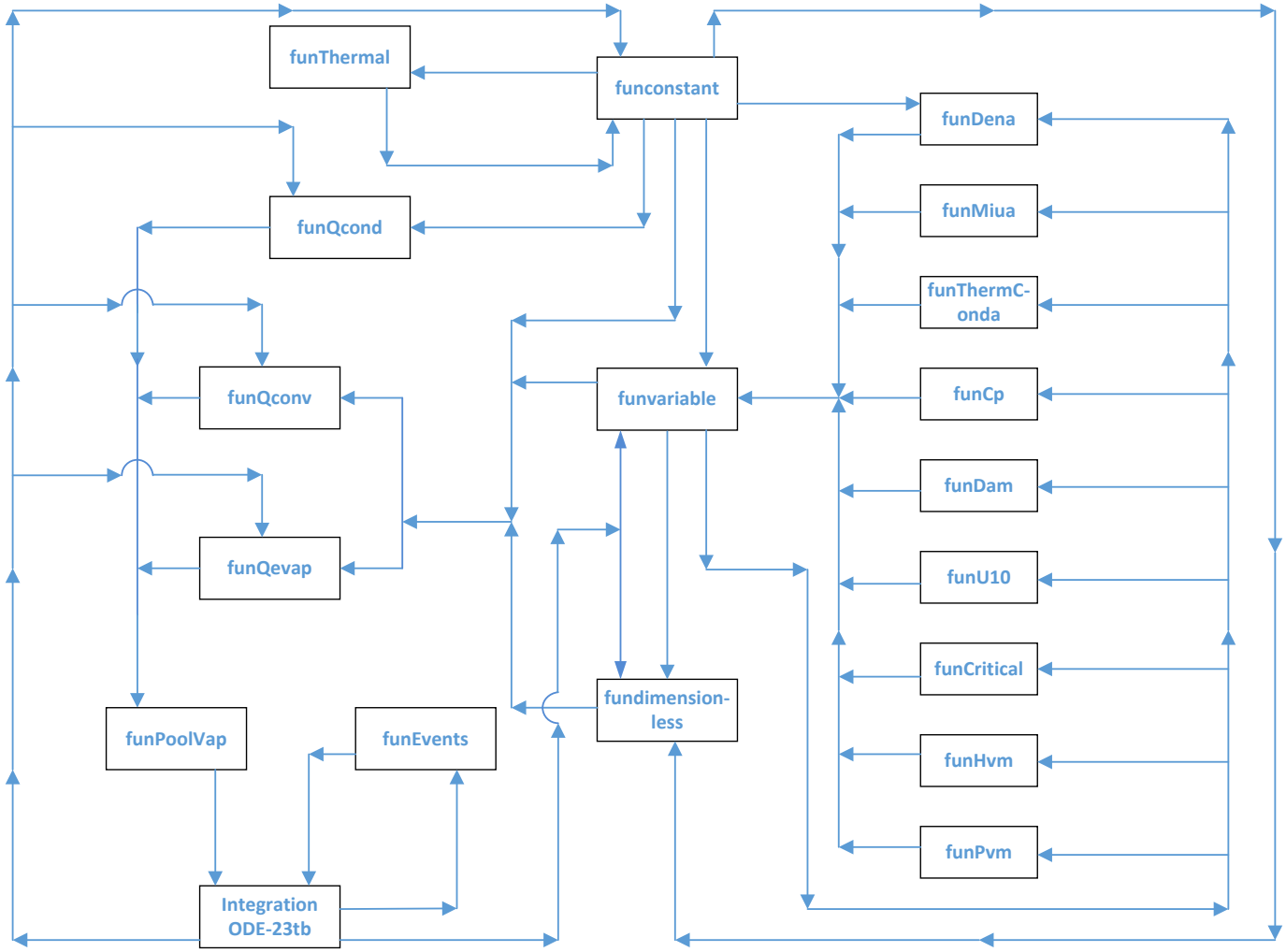
funThermal
funconstant
funDena
funQcond
funMiua
funThermC-onda
funQconv
funvariable
funCp
funDam
funQevap
funU10
funCritical
fundimension-less
funPoolVap
funEvents
funHvm
funPvm
Integration ODE-23tb

Details of the functions are as follow;

funconstant	defines constants for a particular simulation
funvariable	calculates variable parameters
fundimensionless	calculates dimensionless numbers
funDena	calculates the density of air
funMiua	calculates the viscosity of air
funThermConda	calculates thermal conductivity of air
funCp	calculates specific heat capacity of liquid and air
funDam	calculates the diffusion coefficient of liquid in air
funU10	estimates velocity profile
funCritical	provides critical properties of liquid and air
funHvm	calculates latent heat of vaporization of liquid
funPvm	calculates saturated vapor pressure of liquid
funThermal	provides constant thermal properties of substrate
funQcond	calculates conduction heat flux
funQconv	calculates convection heat flux
funQevap	calculates evaporation heat flux
funPoolVap	computes mass and energy balance
IntegrationODE-23tb	carries out integration of mass and energy balance
funEvents	provides event to terminate integration loop

APPENDIX B

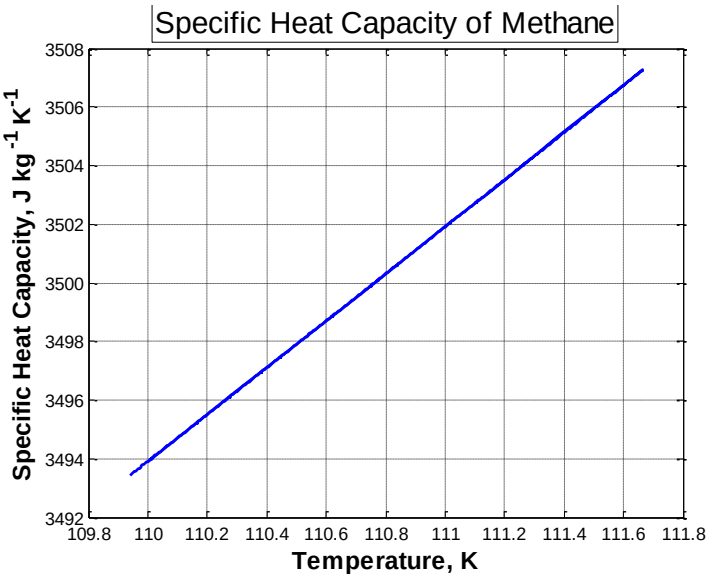

Figure 45: Specific heat capacity of methane

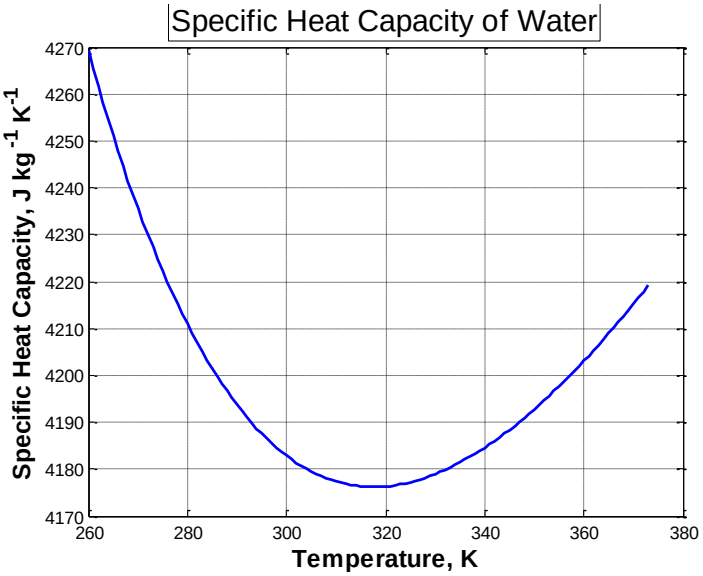

Figure 46: Specific heat capacity of water

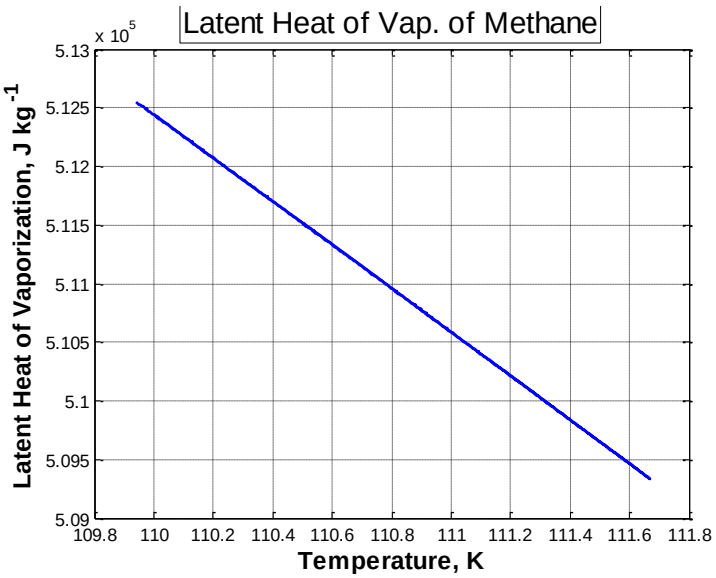

Figure 47: Latent heat of vaporization of methane

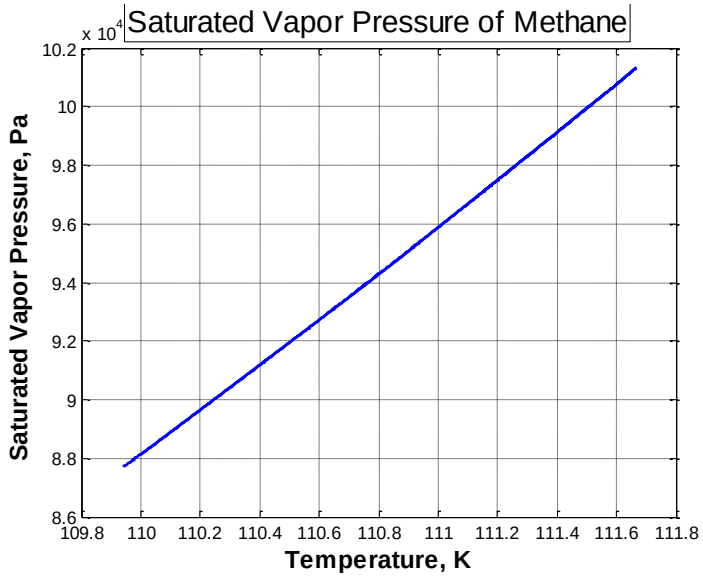

Figure 48: Saturated vapor pressure of methane

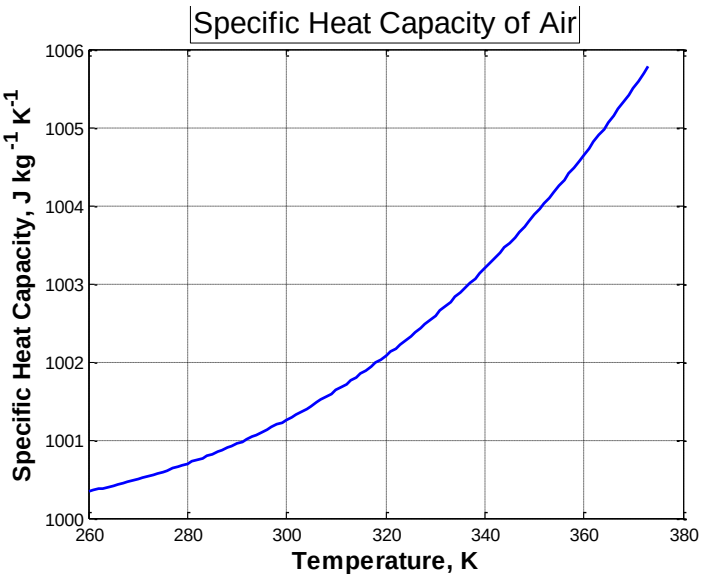

Figure 49: Specific heat capacity of air

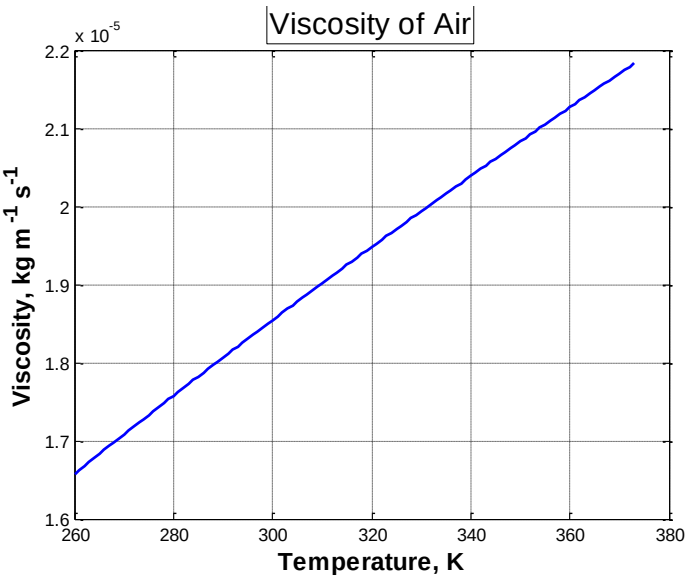

Figure 50: Viscosity of air

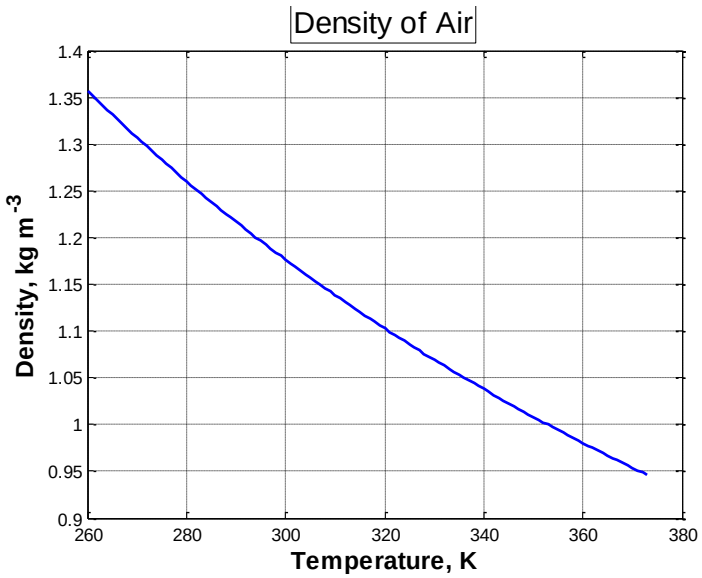

Figure 51: Density of air

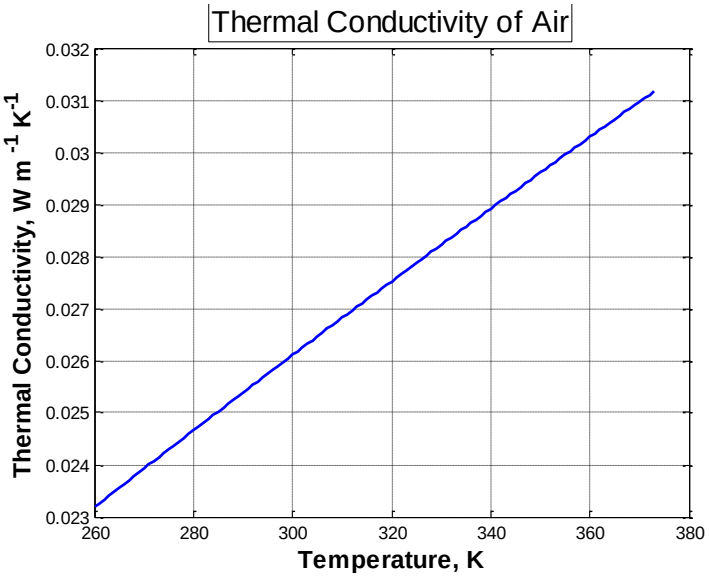

Figure 52: Thermal conductivity of air

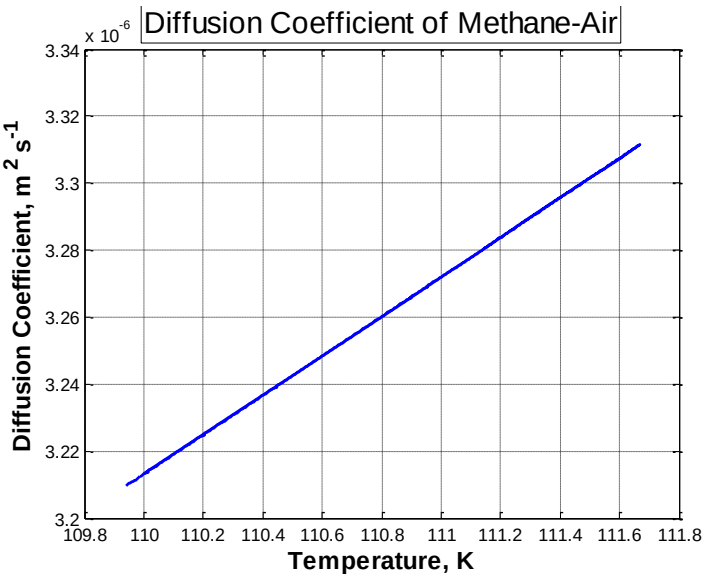

Figure 53: Diffusion coefficient of methane in air